Ultrafast electron diffraction: Excited state structures and chemistries of aromatic carbonyls

Sang Tae Park, Jonathan S. Feenstra, and Ahmed H. Zewail[a)]
Laboratory for Molecular Science, and Physical Biology Center for Ultrafast Science and Technology, California Institute of Technology, Pasadena, California 91125

(Received 23 February 2006; accepted 14 March 2006; published online 4 May 2006)

The photophysics and photochemistry of molecules with complex electronic structures, such as aromatic carbonyls, involve dark structures of radiationless processes. With ultrafast electron diffraction (UED) of isolated molecular beams it is possible to determine these transient structures, and in this contribution we examine the nature of structural dynamics in two systems, benzaldehyde and acetophenone. Both molecules are seen to undergo a bifurcation upon excitation (S_2). Following femtosecond conversion to S_1, the bifurcation leads to the formation of molecular dissociation products, benzene and carbon monoxide for benzaldehyde, and benzoyl and methyl radicals for acetophenone, as well as intersystem crossing to the triplet state in both cases. The structure of the triplet state was determined to be "quinoidlike" of $\pi\pi^*$ character with the excitation being localized in the phenyl ring. For the chemical channels, the product structures were also determined. The difference in photochemistry between the two species is discussed with respect to the change in large amplitude motion caused by the added methyl group in acetophenone. This discussion is also expanded to compare these results with the prototypical aliphatic carbonyl compounds, acetaldehyde and acetone. From these studies of structural dynamics, experimental and theoretical, we provide a landscape picture for, and the structures involved in, the radiationless pathways which determine the fate of molecules following excitation. For completeness, the UED methodology and the theoretical framework for structure determination are described in this full account of an earlier communication [J. S. Feenstra *et al.*, J. Chem. Phys. **123**, 221104 (2005)]. © *2006 American Institute of Physics*.
[DOI: 10.1063/1.2194017]

I. INTRODUCTION

The aromatic carbonyl molecules, exemplified by benzaldehyde and acetophenone, have been of experimental interest for decades. These molecules with close-lying $n\pi^*$ and $\pi\pi^*$ excited states in both singlet and triplet manifolds are ideally suited for the study of the physical processes of intersystem crossing and phosphorescence, as well as photochemical reactions of valence isomerization, bond breakage, and atom transfer. In two recent reports,[1,2] we have presented our preliminary ultrafast electron diffraction results on the photophysical and photochemical channels of benzaldehyde and acetophenone. In this paper, we determine the relevant structures, time scales, and the bifurcation of pathways. We also give a full account of the experimental and theoretical methodologies, and discuss the results and their significance toward the understanding of numerous spectroscopic observations.

A feature shared by both benzaldehyde and acetophenone is a complex manifold of excited states with simultaneous and competitive photophysical and photochemical processes. Ambiguities abound in the pathways, products, and time scales. The mechanisms by which S_2 excited benzaldehyde yields molecular dissociation products while excited acetophenone homolytically cleaves are important issues that portend major advances in understanding excited state decay processes. In order to address the nature of these processes, dark structures of excited state radiationless transitions and chemistries must be determined on the ultrashort time scale.

This paper is outlined as follows: Section II highlights previous spectroscopic findings. In Secs. III and IV the experimental and theoretical frameworks are discussed, respectively. In Sec. V we present the diffraction theory needed and the methodology used for structure determination. In Sec. VI the results of electron diffraction studies on both molecules in their ground states and following 266.7 nm femtosecond excitation to their S_2 states are described, and in Sec. VII we discuss the significance of these findings in the context of the global landscape for bifurcation into photophysical and photochemical processes. First, however, we shall present salient features of the photophysics and photochemistry of the aromatic carbonyls studied here (see Fig. 1).

II. RADIATIVE AND NONRADIATIVE PROCESSES

A. Benzaldehyde

The absorption spectrum of vapor-phase benzaldehyde with wavelengths longer than 260 nm shows two broad peaks. The lower peak is highly structured and corresponds

[a)]Author to whom correspondence should be addressed. Electronic mail: zewail@caltech.edu

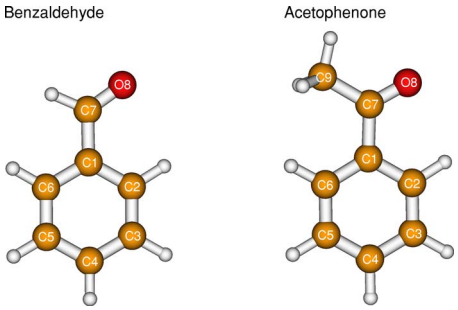

FIG. 1. Molecular structures of benzaldehyde and acetophenone.

to a transition to the S_1 ($n\pi^*$) state. The higher-energy peak, marking transition to the S_2 ($\pi\pi^*$) state, is much more intense and shows only a weak structure.[3] Absorption into either of these states, and the S_3 ($\pi\pi^*$) that lies above, results in phosphorescence.[4,5] This particular feature of benzaldehyde has been exploited by numerous studies attempting an explanation of its photophysics. Experiments to this end have been performed on benzaldehyde in the vapor,[3–20] in solution,[21] and in matrices.[22–24]

The proximity and nature of low-lying $n\pi^*$ and $\pi\pi^*$ states of both singlet and triplet manifolds have been a main focus both experimentally and theoretically. The origin of S_1 ($n\pi^*$) was found to lie 26 919 cm^{-1} above the ground state by sensitized phosphorescence[8] and 26 920 cm^{-1} above by sensitized surface electron ejection.[19] It is slightly blueshifted in hexane solution (26 960 cm^{-1}) (Ref. 21) and in *p*-dibromobenzene matrices (27 284 cm^{-1}).[25] S_2 ($\pi\pi^*$) has its origin at 35 200 and 35 191 cm^{-1} relative to the ground state as seen in the phosphorescence excitation spectrum[11] and ionization excitation spectrum,[13] respectively. Another $\pi\pi^*$ state, S_3, has its 0-0 transition at 41 334 cm^{-1}, as noted by UV absorption.[26] In the triplet manifold, matters are more complex since the $n\pi^*$ and $\pi\pi^*$ states are very close lying. Emission in the vapor is detected only from the $n\pi^*$ (T_1); however, in certain matrix environments the $\pi\pi^*$ may be shifted lower in energy allowing direct spectral observation. The T_1 origin in the vapor phase is readily distinguished by phosphorescence and is assigned between 25 180 and 25 190 cm^{-1}.[8,9,17–19] Similar to the values for the S_1 origin, values for T_1 in liquid hexane[21] and in a *p*-dibromobenzene matrix[25] are blueshifted to 25 195 and 25 515 cm^{-1}, respectively. Some band congestion in the vapor phosphorescence spectrum $\sim$1000 cm^{-1} above the T_1 origin is cautiously assigned to intensity borrowed by the T_2 ($\pi\pi^*$) state.[8,9,17,19] The caution in this assignment arises due to the theoretical suggestion that the spacing between the levels is, in fact, large enough not to cause a significant breakdown of the Born-Oppenheimer approximation.[12,18,27] Theory places the T_1-T_2 energy gap between 726 and 4190 cm^{-1} depending on the method of calculation.[28–31] In matrices, however, the $^3n\pi^*$ and $^3\pi\pi^*$ levels switch and both are observed; the $\pi\pi^*$ state is lower by 162–$\sim$2000 cm^{-1} and varies highly with the choice of host.[23,25]

Decay of the excited state population by phosphorescence is the most widely known relaxation pathway in gas-phase benzaldehyde and the quantum yield of emission approaches unity when excitation is near the S_1 origin.[15] It continues to be observed, albeit with less intensity, as excitation reaches the S_3 state. Two conflicting reports of the phosphorescence behavior at higher excitation energies exist in the literature. In several accounts it is reported that drop-offs in yield occur near both the S_2 and S_3 thresholds.[5,7,12,16] Yet in another account, the drop-offs are refuted as gas-cell "wall effects" and simply a monotonic decrease is reported.[4] Independent of the exact behavior, a nonradiative channel depleting the excited state population becomes important above S_1 excitation making phosphorescence less significant. An intermediate state invoked in the nonradiative decay route lives long enough for collision-induced deactivation as added gas causes an increase in phosphorescence yield.[7,11,12,14,16] The phosphorescent state itself is found to live in the range of milliseconds to nanoseconds, shortening with increased excess energy.[4,10,14,19] Lifetime information is also available for the S_2 state by femtosecond photoelectron spectroscopy. It was observed to live for 440 fs at the origin and undergoes a monotonic lifetime decrease with increasing excitation energy, leaving the state by ultrafast internal conversion.[20]

The structures of the electronic states of benzaldehyde are largely obtained through theoretical means[29–31] with some experimental exceptions. The ground state has been studied by both microwave spectroscopy[32] and electron diffraction[33] in the gas phase, and the barrier to formyl group torsion is found to be 1715 and >1700 cm^{-1}, respectively. Additionally, analysis of the phosphorescence spectra and S_1 excitation spectra shows the C=O stretch as the most intense band with prominent progression, confirming the $n\pi^*$ nature of both states as well as their structural similarity to the ground state (except for the C=O length).[8]

In addition to the rich photophysics studied in this molecule, there exist chemical pathways resulting in radical and molecular dissociation products. The first thorough experiments on the photochemistry of benzaldehyde[11] show dissociation into benzene and carbon monoxide upon photolysis by 276 nm radiation (S_2 excitation). The products were extracted from the cell and identified by gas chromatography. Being relatively insensitive to added oxygen, the molecular dissociation products are determined to have formed through a "concerted" reaction and not through radical intermediates. At low pressures the quantum yield of benzene is found to be 0.89, and the addition of foreign gases causes the benzene yield to decrease while increasing the yield of phosphorescence. A model is proposed with short and long benzene formation channels; the long channel may be deactivated to the phosphorescent state (T_1) by collisions.[11] An insensitivity to collisions with added O_2 further supports the nonradical nature of the reaction, as the yield of benzene was unchanged.[6] The nature of the reaction was conclusively verified in experiments where benzaldehyde-d_6 was mixed with the benzaldehyde-h_6 and photolyzed with 276 nm radiation.[12] Only the concerted intramolecular reaction products benzene-d_6 and benzene-h_6 were identified. Yield of the dissociation products was near unity.[12] Benzene ion has also been detected in mass spectrometry experiments pumping at 248 nm.[34]

Although ultrafast dynamics was hitherto lacking, some time scales of benzene formation have been obtained. In an ionization experiment using single shots of 2 ns pulses,[35] benzene ions were detected with 258.9 nm excitation but not with 258.7 nm. For both excitations benzene is formed within the pulse, but because ground state benzene has a resonant absorption at 258.9 nm, but not at 258.7 nm, it is efficiently ionized and observed at 258.9 nm. Furthermore, the photoelectron spectrum was recorded at both excitation energies for benzaldehyde as well as benzene. No photoelectrons were detected at 258.7 nm, but the spectrum observed using 258.9 nm matched that of ground state benzene. In addition to confirmation of the product, these experiments put an upper bound of 2 ns on the photoreaction.[35] In another report, single shots at 266 nm showed no benzene ion signal when the pulse width was 25 ps, but showed a near-unity production of benzene ions when the excitation laser pulse width was 8 ns.[36,37]

Using 10 ns pulses at 266 nm in a mass spectrometer Polevoi *et al.* determined the time constant for benzene ion formation to be ~30 ns. Their kinetic model predicts that the reaction corresponds to triplet benzaldehyde dissociating into benzene in its own triplet state and ground state carbon monoxide.[38] The most recent work on benzaldehyde photochemistry by Silva and Reilly, a time-resolved mass spectrometry study using 3–5 ns pulses, contributes valuable additional information.[39] With excitation into S_2 and time delayed photoionization by the 157 nm probe laser, both benzene and parent benzaldehyde ions are detected. The ratio of benzene to benzaldehyde ions increases with a decreasing excitation wavelength—complete dissociation occurring near 260 nm excitation. Two decay times are observed for the benzaldehyde ion: a short decay of <1 μs and a longer decay of >1 μs. The shorter decay time nearly coincides with the time constant of benzene ion appearance and is ~80 ns at 270 nm excitation. Since the probe pulse (157 nm) is only intended to ionize electronically excited benzenes, the benzene ion signal is believed to be from the triplet. However, ground state benzene is also identified in their results by its photoionization excitation spectrum and must be formed via a different pathway. The threshold for benzene formation is placed somewhere near (but below) the S_2 origin.[39]

Radical products were reported only once from S_2, after gas phase photolysis of benzaldehyde by 7 ns pulses of 280, 285, and 308 nm radiations. HCO radicals were detected by absorption and quantum yields were estimated at 0.3–0.4.[40] Based on the evidence in numerous previous works, the radicals must surely be products of a multiphoton reaction. The chemistry observed upon excitation into the S_2 state contrasts with the different chemistries observed through S_1. Several researchers report no chemistry at all after S_1 excitation.[4,12,14,36,37] Chemistry that is reported is of a fragmentation nature resulting in the benzoyl radical and atomic hydrogen.[22,41] One study notes a slow buildup of polymer on the walls of the gas cell after prolonged exposure at 328 or 365 nm.[11] Hydrogen atoms were also produced in the thermal breakdown of benzaldehyde above 1000 K. CO may also be lost from the resulting fragment above 1150 K.[42]

B. Acetophenone

The states of acetophenone are similarly ordered as benzaldehyde, with two close-lying triplet states (the lower one being strongly phosphorescent) located just below the S_1 origin. There are many experimental measurements and theoretical estimates of the relative energies of the states in the gas phase. S_1 ($n\pi^*$) is found to lie 27 279 cm^{-1} above S_0 by its sensitized phosphorescence.[8] The origin of the S_2 ($\pi\pi^*$) excitation spectrum is 35 402 cm^{-1} above S_0 (Ref. 43) and the 0-0 by optoacoustic spectroscopy is reported at 34 010 cm^{-1}.[6] The S_3 ($\pi\pi^*$) origin is seen at 41 695 cm^{-1} by absorption in a jet.[26] In the triplet manifold, the well-known T_1 ($n\pi^*$) state has its origin at 25 791 cm^{-1} by sensitized phosphorescence[8] and 25 786 cm^{-1} by its direct emission.[44] Like benzaldehyde, the T_2 ($\pi\pi^*$) state was not directly observed in the vapor. A congestion of spectral features noted 600 cm^{-1} above the T_1 origin has been attributed to possible mixing with the nearby T_2.[8] In general, the vapor-phase spectrum is weaker than that of benzaldehyde, with a less prominent progression of the carbonyl stretching bands—perhaps from a greater contribution of $\pi\pi^*$ character.[9] Unlike benzaldehyde, emission from only a single phosphorescent site is observed in certain matrices and believed to correspond to some highly perturbed state. Indeed, the spectrum shows features from both states precluding it from being unequivocally assigned to either the $^3n\pi^*$ or $^3\pi\pi^*$. The conclusion is that the T_1-T_2 energy gap is even less than that of benzaldehyde.[23,44] The energies and geometries of these low-lying electronic states have been studied theoretically, yielding similar results. An estimate of the T_1-T_2 energy gap is only 565 cm^{-1}.[30,31]

Like for benzaldehyde, the prolific study of acetophenone is largely due to its intense phosphorescence facilitated by efficient intersystem crossing from S_1 into the triplet manifold. The photophysics of acetophenone have been studied in the gas phase,[6–9,20,26,43–47] solution,[21,48] and in matrices.[22,23,44] Phosphorescence detected in the vapor phase is seen to decrease in intensity with increasing photon energy and exhibits a drop-off as excitation approaches S_2. The phosphorescence quantum yield at the S_1 origin is near unity,[7,45,47] while at the S_2 origin it is reduced to ~10^{-4}.[43] The drop-off is attributed to the rise of an intermediate state that can be collisionally deactivated—increased phosphorescence yield is observed with the addition of foreign gas.[7,45,47] A kinetic model predicts a lifetime of 380 ns for the intermediate.[7] Again, like benzaldehyde, the presence of a drop-off is contested with contrary evidence depicting a monotonic decrease.[47]

Although phosphorescence lifetimes are known to be in the microsecond to nanosecond range, the lifetimes of other states have gone largely unmeasured. By linewidth measurements the lifetime of the S_2 origin is found to be 260 fs,[43] and a subsequent femtosecond time-resolved photoelectron experiment puts it at 140 fs, faster than that of benzaldehyde. The faster decay is likely the consequence of more efficient radiationless relaxation mediated by extra accepting modes from the methyl group.[20] The lifetime of the Rydberg state reached by 193 nm absorption is instrument limited and

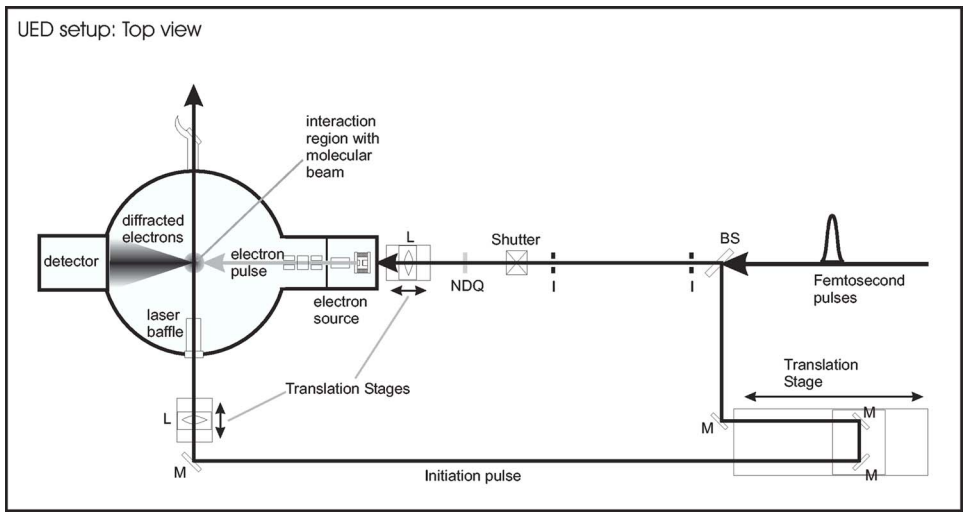

FIG. 2. Schematic diagram of the UED setup. The output of the amplified femtosecond laser system is split such that a majority of the power is time delayed and used to initiate the reaction in the molecular beam. The weak light pulses produce electron pulses which intersect the pump laser and molecular beam in the diffraction chamber. Diffracted electrons generate signal on a digital detector.

<200 fs.[49] These fast lifetimes and the experimentally known (and theoretically predicted)[30] efficiency of intersystem crossing are consistent with the lack of fluorescence from acetophenone. Fluorescence has been observed, however, from acetophenone derivatives in solution with attached aromatic groups.[50]

Experimental information regarding the structures of the excited states is confined to the S_1 and T_1 states. The carbonyl stretching progression observed is indicative of $n\pi^*$ states with the main structural difference from the ground state being a lengthening of the C=O bond.[8] Experimental information on the $\pi\pi^*$ structures is limited to acetophenone derivatives where the $^3\pi\pi^*$ state is lower in energy. Substituted acetophenones were excited in solution with 266 nm light after which (500 ns) infrared spectra were recorded. The changes in the spectrum indicate a structural difference with the ground state mainly in the aromatic ring consistent with the quinoid structure of a $\pi\pi^*$ state.[51] Theoretical inquiries back up these experimental results reaffirming structural differences with the ground state localized in the C=O bond for $n\pi^*$ states and in the aromatic ring for $\pi\pi^*$ states.[30,31] It is to be noted that no experimentally determined structure exists for ground state acetophenone.

Acetophenone photochemistry has attracted less interest than that of benzaldehyde. Unlike the molecular dissociation seen in the aldehyde, radical products represent the photochemistry of this aromatic ketone. Carbon monoxide was not detected in the earliest of experiments by Berger and Steel.[45] Instead, the major products are the benzoyl and methyl radicals observed at multiple excitations ranging from 282 to 193 nm and also seen as products in strong-field dissociation experiments. The other radical cleavage products, phenyl and acetyl radicals, are also observed but with a much lower yield.[45,52,53] Like benzaldehyde, the yield of chemical products is seen to approach unity with S_2 excitation at the lowest pressures but decreases coincident with increasing phosphorescence when foreign gas is added, suggesting a vibrationally excited intermediate to fragmentation. Only trace amounts of the molecular dissociation products of carbon monoxide and toluene were detected after photolysis by 193 and 248 nm radiations; a branching ratio with the radical products of $\sim 1:100$.[53] Little to no decomposition products are noted upon S_1 (365 nm) excitation.[45]

III. EXPERIMENT

The third-generation ultrafast electron diffraction apparatus at Caltech has been briefly presented elsewhere,[54,55] and here we provide the detailed methodology that makes these experiments possible. The ultrafast electron diffraction (UED) experimental apparatus is a combination of several components that will be addressed separately: a femtosecond laser system, a high-vacuum chamber, a high-voltage ultrafast pulsed electron gun, a charge-coupled device (CCD) detector, and a high-temperature inlet system. Simply summarized, the beam from the femtosecond laser system is split and the more intense pulses are focused and directed into a molecular beam to initiate reaction. The weaker femtosecond laser pulses are focused onto a back-illuminated silver photocathode in the electron gun to generate electron pulses by the photoelectric effect. The pulses are accelerated and focused to meet the excitation laser and the molecular beam in a mutually perpendicular arrangement. Scattered electrons are detected by a CCD camera at the terminus of a phosphor, fiber-optic, image-intensifier chain. The excitation laser pulses may be delayed to provide time-dependent diffraction patterns. A schematic drawing of the setup is shown in Fig. 2.

Samples used in these experiments were obtained from Aldrich: acetophenone (99%), benzaldehyde (99.5+%), and 1,3-butadiene (>99%), and Air Liquide: carbon dioxide (99.5%) and xenon (99.995%). All samples were used without further purification.

A. Femtosecond laser system

The laser system used in these UED experiments is a mode locked Ti:sapphire oscillator (Tsunami) which delivers pulses (6 nJ; 800 nm; 60 fs; 80 MHz) to a dual-stage Ti:sapphire amplifier (Super Spitfire). Amplified pulses (2.3 mJ, ~120 fs, 800 nm; 1 kHz) are frequency tripled in a third-harmonic generator module (Uniwave) to provide ultraviolet

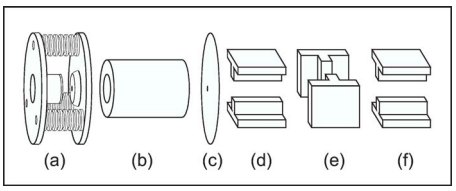

FIG. 3. Elements of the pulsed electron source. Femtosecond laser pulses enter the electron source from the left. The photocathode and anode (a) are separated by 3 mm and experience a potential of 30 kV. Electrons pass through a hole in the anode and are focused by the magnetic lens (b). The electron source is separated from the scattering chamber by a 2 mm aperture (c). Vertical (d) and horizontal (e) deflection plates and vertical streaking plates (f) are used to adjust the electron beam position and to measure its temporal width.

pulses (400 μJ; 266.7 nm). The UV beam then enters the "optics table" (see Fig. 2) where it is split into electron-generation and excitation pulses. The electron-generation beam (~7% of the original beam) passes through two irises closed to ~1 mm to attenuate the beam and improve its transverse mode. The beam also passes through an NDQ100 (10% transmission) neutral density filter for further attenuation. A lens with a focal length of 300 mm then focuses the beam into the electron gun. The significant attenuation of the electron-generation beam is necessary to prevent damage to the photocathode which must maintain its integrity for the duration of the experiment. A computer controlled, modified camera shutter prevents electron extraction except during data acquisition.

The excitation beam (93% of the original beam from the tripler) is time delayed by a translation stage before it, too, is focused by a movable lens into the diffraction chamber. The translation stage has a range of approximately 1.5 ns; a laser pulse can arrive in the scattering chamber ~1 ns before an electron pulse.

B. Ultrafast electron system

The pulsed electron gun (Fig. 3) is housed in a chamber separated from the diffraction chamber by a 2 mm aperture. The chamber is pumped by a BOC Edwards turbomolecular pump (EXT 250; ~200 l/s) by which pressure is maintained at $\sim 10^{-7}$ torr during experiments (nearly independent of molecular beam operation). Before entering the chamber, laser pulses pass through two irises (each at ~1 mm) and a NDQ100 (10% transmittance) to attenuate the beam such that the photocathode is not damaged over the course of the experiment. Laser pulses are focused with an adjustable lens and enter the chamber to impinge on a back-illuminated photocathode. The photocathode consists of a stainless steel mount to which a sapphire window is fastened by silver paste. A silver coating of 25 nm is deposited on the window using a BOC Edwards Auto 306 vacuum coater.

A voltage of 30 kV is maintained via high-voltage feedthrough and a high-voltage power supply and a grounded extraction anode is positioned 3 mm from the coated surface by ridged Macor spacers. The electron beam passes through a 200 μm pinhole on the extraction anode to clean the profile. Accelerated electrons have $\lambda_{\text{de Broglie}} = 0.06979$ Å [see below, Sec. V B, Eq. (5)] and are traveling at 9.8×10^7 m/s (nearly 1/3 the speed of light). Leaving the extraction region, electrons are focused with an electromagnetic coil by which the size and shape are optimized [~400 μm full width at half maximum (FWHM) with Gaussian profile]. The electrons then pass through the 2 mm pinhole separating the electron gun chamber from the scattering chamber. Once in the scattering chamber, two sets of deflection plates (horizontal and vertical) and a set of streak plates (vertical) are used to manipulate the electron beam's path and its final position on the detector. The streak plates are used in the streaking experiments that measure the temporal profile of the electron pulses. In addition, they are also needed to move the beam outside of the filtered region on the detector (see below) where the number of electrons present in a single pulse may be measured accurately.

Calibrations have been performed relating the temporal pulse width to the number of electrons per pulse so that streak measurements do not have to be performed prior to every experiment.[54] The pulse properties for these experiments were measured to be 8×10^4 electrons/pulse for acetophenone and 3×10^4 electrons/pulse for benzaldehyde. The FWHMs of the electron beams were measured to be ~370 and ~360 μm for benzaldehyde and acetophenone, respectively, and the pulsewidths in these experiments were typically less than 6 or 20 ps depending on the number of electrons per pulse.

The photocathode must undergo a period of "warming up" where the number of electrons increases over time with exposure of the photocathode to the laser. This typically takes 12 h, after which the beam is stable and ready for diffraction experiments.

C. Diffraction chamber and molecular beam

The scattering chamber is separated from its primary pumping system (Varian VHS-6 oil diffusion pump, 2400 l/s, with a liquid nitrogen baffle) by a pneumatic gate valve. The pump permits vacuum to 10^{-7} torr when the molecular beam is not running. Pressures during the experiment can be as high as 3×10^{-4} torr. Electron scattering from background gas is minimized by the use of a liquid nitrogen cryotrap which is a baffle (Varian) attached to the diffusion pump.

Stray excitation laser light in the scattering chamber is minimized by a baffle that extends approximately 10 cm from the CaF_2 inlet window. After many hours of experimentation with certain organics, background gas can lead to the formation of a layer of polymeric coating on the inlet window and this reduces the laser transmission. After crossing the molecular and electron beams in the interaction region, excitation laser light exits the chamber through a quartz window at Brewster's angle. The top view schematic of the scattering chamber is shown in Fig. 2.

The inlet manifold was rebuilt prior to the experiments on benzaldehyde and acetophenone in order to accommodate their high boiling points. The current inlet is constructed entirely of stainless steel. A sample reservoir is capable of holding 300 ml of sample and the valves can tolerate heats of up to 400 °C. A manifold is connected to the high-temperature

portion of the inlet through a fine-metering needle valve. The manifold allows CO_2, Xe, and butadiene access to the nozzle. The manifold is also connected to a mechanical pump for evacuation during sample changes.

The nozzle tip, with a 180 μm aperture, is connected to the manifold via a stem running through an insulated flange. The nozzle (and stem) is heated by a tight wrap of an insulated high-resistance thermocouple wire, the manifold is wrapped in a fiberglass heating tape, and the reservoir is clamped with a custom band heater (Watlow). The heating systems of each unit are monitored and controlled separately. The temperatures are optimized to prevent condensation clogging and thermal decomposition while still delivering an appropriate amount of sample to the interaction region. Vaporized sample from the reservoir passes through the manifold, stem, and nozzle to form a molecular beam via effusive expansion. For benzaldehyde the temperatures of the nozzle, manifold, and sample were 210, 230, and 129 °C, respectively. The temperature of the sample reservoir was increased to 148 °C over the course of the experiment in order to keep constant the pressure and the dependent scattering signal. For acetophenone the temperatures of the nozzle, manifold, and sample were 230, 260, and 110 °C, respectively, and the sample temperature was increased to 120 °C during this much shorter experiment.

The size of the molecular beam is measured by admitting gas (CO_2) to the chamber and moving the nozzle across the stationary electron beam. The scattering intensity at each nozzle position is plotted and fitted with a Lorentzian curve. The width of the electron beam is deconvoluted to yield the molecular beam width. The nozzle must be 800–900 μm above the electron beam for a molecular beam width similar in size to those of the laser and electron beams. The molecular beam sizes for the benzaldehyde and acetophenone experiments were measured to be 380 and 270 μm, respectively.

D. Clocking and zero of time

Optimizing the overlap between the electron, laser, and molecular beams in the scattering chamber and determining the temporal relationship between electron and laser pulses are done simultaneously. Rough overlap optimization of the molecular beam with electron beam and laser beam is aided by the shadow cast by the nozzle and viewed on the CCD and through the outlet window, respectively. Overlap is fine-tuned by observing and maximizing a photoion-induced lensing effect on the electron beam.[56] Gas (1,3-butadiene) is delivered to the scattering chamber via the inlet nozzle and the laser and electron beams are admitted to intersect with it. The undiffracted electron beam profile is monitored while the time delay of the laser pulses is changed. The laser causes ionization of the gas and the subsequent charge separation alters the shape of the transmitted electron beam. The time at which the electron beam shape begins to change from circular to elliptical give the *in situ* time zero.[56] The position of the laser is fine-tuned using the inlet mirror and focusing lens to maximize the lensing effect.

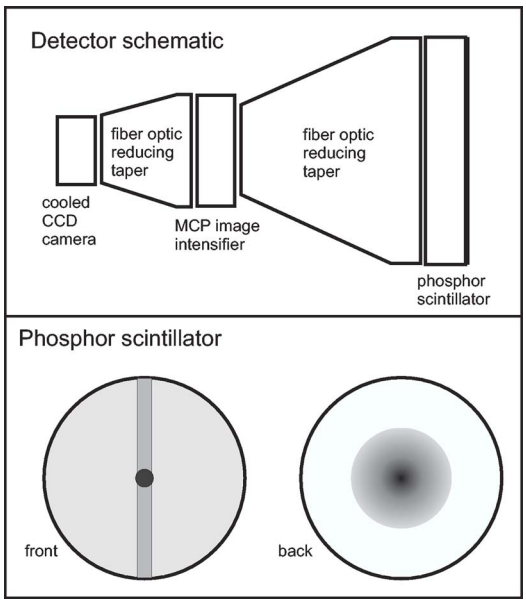

FIG. 4. (top) Side view of the detector schematic. (bottom) Front and back views of the phosphor screen showing the vertical null stripe and central beam stop and the phosphor-coated face plate with the radial symmetric filter.

The overall experimental time resolution is governed by the laser pulse width, the electron pulse width, and the group velocity mismatch. Using the above-mentioned beams' properties and published formulas,[54,57] the overall time resolutions of the benzaldehyde and acetophenone experiments were derived.

E. Detector and data acquisition

Detection of the electron diffraction signal is done with a CCD camera at the end of an image-intensifier fiber-optic chain (see Fig. 4). The phosphor scintillator is comprised of a fiber-optic disk (diameter=8 cm) with a coating of P-47 phosphor. A 300 nm layer of aluminum is applied to block any scattered UV light. A radial symmetric neutral-density filter is coated on the reverse side of the fiber-optic disk in order to increase the dynamic range of detection (the electron diffraction signal decreases rapidly with a scattering angle). Electrons strike the phosphor screen and emit photons which then travel through the disk and the fiber-optic reducing taper to the image intensifier (Hamamatsu) which amplifies the signal via a microchannel plate. The output photons traverse a second fiber-optic reducing taper and are detected by a CCD camera (Photometrics, KAF-1000). The CCD camera is cooled to −40 °C in order to reduce noise. The entire setup is capable of single electron detection (~100 detector intensity units/electron). The CCD camera consists of a 1024 × 1024 pixel array. The effective pixel size is 57.8 μm on the side of the phosphor screen, and pixels are binned 2 × 2 during the experiments.

Since the vast majority (~99%) of the electron beam passes through the molecular beam unscattered, a small metal cup mounted on an aluminum strip covers the center of the phosphor scintillator to prevent saturation of the detector. In addition, the image-intensifier itself has a null stripe bi-

secting along the vertical, separating the left and right halves which can be operated separately. Exposure of the CCD and data acquisition is entirely computer controlled. The standard exposure time is 240 000 pulses (4 min). Multiple exposures (typically 100) are acquired and averaged in the data processing (see below).

One hundred diffraction patterns (4 min exposures at 1 kHz) are taken for each of background electron scattering (no molecular beam), carbon dioxide, xenon, ground state (molecular sample without excitation laser), each time-resolved benzaldehyde data point (−100, −50, −10, −5, +0, +5, +10, +15, +20, +30, +40, +50, +100, and +1000 ps), and each time-resolved acetophenone data point (−100, +50, and +100 ps). Conversion of the pattern data to the scattering intensity curves used in the data analysis will be dealt with in detail in Sec. V.

IV. STRUCTURE QUANTUM CALCULATIONS

Structural refinement in UED requires an initial guess geometry. Although one could, in principle, use a chemically intuitive guess, our data analysis is always begun with the structural results of *ab initio* or density functional theory (DFT) calculations. Ideally, regardless of the choice of initial guess, structural refinement should converge to one single true structure. In practice, however, this is not always true, especially when there are a large number of structural parameters involved and the fitting surface contains many local minima. Therefore, it is a good practice to have an initial guess as close to the true structure as possible. For this, a high level of theoretical calculation is desired, such as DFT, coupled cluster (CC), quadratic configuration interaction with single and double excitations (QCISD), or multiconfiguration self-consistent field (MCSCF). In our study, all calculations have been carried out using either GAUSSIAN98 (Ref. 58) or GAMESS (Ref. 59) packages. The details of data analysis and structural refinement in UED are covered in Sec. V.

A. Ground state

For the structures of molecules in the singlet (S_0) or triplet (T_1) ground states, highly accurate results are available at fairly low computational costs. The B3LYP level[60] with the 6-311G(d,p) basis set has been found useful in determining structure, energy, and vibrational frequencies.[54,61]

Geometry optimization for the ground state of reactants and possible products of benzaldehyde and acetophenone systems were carried out at the B3LYP level using the 6-311G(d,p) basis set. UB3LYP/6-311G(d,p) was used for radical product candidates such as those involving H, methyl, formyl, acetyl, benzoyl, and phenyl radicals as well as for the triplet state of molecules. Planar symmetry was imposed for the singlet ground states of benzaldehyde and acetophenone and the T_1 state of benzaldehyde, and frequency calculations were performed to ensure minimum energy configurations. For the T_1 state of acetophenone, the symmetry constraint was lifted, since the methyl orientation deviates from planar symmetry; the skeleton remains nearly planar. The theoretically determined relative energies of the parent and product molecules are listed in Table I and compared to experimental values where available; the agreement is satisfactory. Experimental values of the changes in heats of formation at 298 K were taken from NIST (Ref. 62) and then converted to 0 K values using the theoretical frequencies obtained from DFT calculations.

B. Excited state

Several methods are available for calculating the properties of excited states. Among them, MCSCF uses a minimum set of orbitals (active space) for a configuration interaction (CI) calculation; just enough to determine the relevant excited state characteristics.[63]

MCSCF calculations were performed for singlet and triplet, ground and excited states, of benzaldehyde and acetophenone to explore structural changes during the photophysical processes. An active space was chosen to account for the carbonyl $\pi^* \leftarrow n$ and phenyl $\pi^* \leftarrow \pi$ transitions in both molecules. Specifically, ten electrons were partitioned into nine orbitals: one oxygen nonbonding orbital, one each of C=O π and π^* orbitals, and three each of C=C π and π^* orbitals. The 6-31G(d) basis set was used to reproduce previous work on benzaldehyde by Wang *et al.*[31] Following this confirmation, calculations were then conducted using the 6-311G(d,p) basis set. The initial molecular orbitals were guessed from the B3LYP calculations with virtual orbital optimizations after SCF convergence. Using the guessed orbitals, which were properly reordered to form nine active spaces, vertical energies were calculated and molecular orbital characters were visually checked to confirm the corresponding transitions observed in the experiments. Full structural optimizations were followed by vibration frequency calculations to check the effect of imposing planar symmetry. Multireference perturbation corrections (MCQDPT) (Ref. 64) were applied to evaluate the electron correlation energies. Relative energies of excited states are listed in Table II and compared with experimental values where available.

In calculating reactive pathways from the $n\pi^*$ S_1 excited state of benzaldehyde, the SCF suffered convergence failure; the selected initial guess wave functions do not remain effective when large nuclear coordinate changes are implemented.[65] For unknown reasons, preparing the initial guess vector at the rearranged geometry was also unsuccessful. Since the S_1 MCSCF reaction pathway calculations failed, UB3LYP/6-311G(d,p) was employed to study the reaction on the $n\pi^*$ T_1 surface instead. Both the S_1 $^1n\pi^*$ and T_1 $^3n\pi^*$ states of acetophenone and benzaldehyde have nearly identical stationary geometries and vibrational frequencies. The similarities permit results found for T_1 benzaldehyde to be carefully adapted to the S_1 surface; a correction of 3906 cm^{-1} is used, the difference between the experimental S_1 origin and the DFT T_1 origin. Later discussion of the S_1 dynamics is made under the assumption that calculations on T_1 provide information relevant to its singlet counterpart.

TABLE I. Theoretical and experimental energetics of benzaldehyde and acetophenone: chemistries.

		Energy (cm^{-1})		
Molecule	Channel	Theor.[a]	Expt.[b]	Temperature[c] (K)
Benzaldehyde	C_6H_5CHO (S_0^*)	0	0	2379
	C_6H_5CHO (T_1)	23 015	25 183	1307
	C_6H_5CHO (T_2)	25 148	25 183 ~ 26 183	1161
	C_6H_6 (S_0)+CO	840	460	2696
	C_6H_6 (T_1)+CO	30 489	30 087[d]	1044
	H+C_6H_5CO	30 403	n/a[e]	954
	C_6H_5+HCO	32 335	34 637	993
Acetophenone	$C_6H_5COCH_3$ (S_0^*)	0	0	2058
	$C_6H_5COCH_3$ (T_1)	23 569	25 791	1157
	$C_6H_5COCH_3$ (T_2)	25 643	n/a[e]	1068
	$C_6H_5CH_3$ (S_0)+CO	1 860	1 814	2227
	$C_6H_5CH_3$ (T_1)+CO	30 662	30 890[f]	945
	CH_3+C_6H_5CO	26 660	n/a[e]	1284
	C_6H_5+CH_3CO	31 200	34 266	972

[a]Theoretical energies were evaluated from B3LYP/6-311G(d,p) level calculations, except for the energies of the T_2 states of benzaldehyde and acetophenone which were evaluated using MCSCF(10,9)/6-311G(d,p).
[b]Experimental values were evaluated from the change in the heat of formation at 298 K (Ref. 62) and converted to the 0 K value using DFT frequencies.
[c]Temperatures for dissociation products are upper limits where all the excess energies are partitioned into vibrational energy; none for relative translational energy and rotational energy.
[d]The energy of C_6H_6 ($^3B_{1u}$) is 29 627 ± 12 cm^{-1} by mass-analyzed threshold ionization (MATI) of discharged benzene (Ref. 79). The energy of C_6H_6 ($^3B_{1u}$) is 3.665 eV from electron-energy-loss (EEL) data (Ref. 80).
[e]These data were not available.
[f]The energy of $C_6H_5CH_3$ (T_1) is 3.605 eV (0-0) for the solid (Ref. 81) and 3.8 eV (maximum) for the gas (Ref. 82).

V. DIFFRACTION THEORY AND METHODOLOGY

A. 2D diffraction patterns and the detector function

As mentioned in Sec. III E, a spatial filter on the back side of the phosphor scintillator increases the dynamic range of detection by leveling the rapid drop-off of scattering intensity. However, this effect must be accounted for in order to obtain the molecular scattering function. The experimental raw patterns, F^e, containing the filter effect, $\eta(x,y)$, can be expressed as

$$F^e(x,y) = I^e(x,y) * \eta(x,y), \tag{1}$$

where I^e denotes the experimental two-dimensional (2D) intensity at detector pixel (x,y). I^e is the sum of the sample

TABLE II. Theoretical and experimental energetics of benzaldehyde and acetophenone: excited states.

		Benzaldehyde			Acetophenone		
		Expt.[a]	MCSCF[b]	MCQDPT[b]	Expt.[c]	MCSCF[b]	MCQDPT[b]
S_0		0	0	0	0	0	0
S_1	($^1n\pi^*$)	26 921	26 541	27 370	27 279	⋯ (26 703)[d]	⋯ (27 278)[d]
S_2	($^1\pi\pi^*$)	35 191	35 978	33 028	35 402	36 074	33 329
T_1	($^3n\pi^*$)	25 183	24 844 (24 766)[d]	24 976 (24 899)[d]	25 791	25 556 (25 542)[d]	25 622 (25 514)[d]
T_2	($^3\pi\pi^*$)		24 821	25 148		25 102	25 643
T_3	($^3\pi\pi^*$)					36 361	32 639

[a]For benzaldehyde, the S_1 origins are 26 919 cm^{-1} (Ref. 8) 26 920 cm^{-1} (Ref. 19), and 26 921 cm^{-1} (Ref. 17). The S_2 origins are 35 200 cm^{-1} (Ref. 11) and 35 191 cm^{-1} (Ref. 13). The S_3 origin is 41 334 cm^{-1} (Ref. 26). The T_1 origins are 25 180 cm^{-1} (Ref. 18), 397 nm (Ref. 10), 25 184 cm^{-1} (Ref. 9), 25 183 cm^{-1} (Ref. 8), 397 nm (Ref. 19), and 25 183 cm^{-1} (Ref. 17).
[b]MCSCF and MCQDPT calculations were performed using the 6-311G(d,p) basis set and an active space of ten electrons partitioned in nine orbitals.
[c]For acetophenone, the S_1 origin is 27 279 cm^{-1} (Ref. 8). The S_2 origins are 35 402 cm^{-1} (Ref. 43), and 34 010 cm^{-1} (Ref. 6). The S_3 origin is 41 695 cm^{-1} (Ref. 26). The T_1 origins are 25 791 cm^{-1} (Ref. 8), and 25 786 cm^{-1} (Ref. 44).
[d]Values in parenthesis are for structures which the planar symmetry is imposed and results in an imaginary frequency.

scattering signal (I) and the background scattering (I^b). The latter, in principle, is the result of scattering due to the background gas (I^a), laser (I^l), and the detector (I^d). In order to eliminate the filter function, we simply measure the scattering of monoatomic Xe, $F^e_{\mathrm{Xe}}(x,y)$, which generates a smooth monotonic signal, and measure the contribution of the detector's noise, $F^d(x,y)$, which is recorded in the absence of sample and the laser. It is then straightforward to eliminate the filter function by defining the following ratio:

$$R^e(x,y) = \frac{F^e(x,y) - F^d(x,y)}{F^e_{\mathrm{Xe}}(x,y) - F^d(x,y)} = \frac{I^e(x,y) - I^d(x,y)}{I^e_{\mathrm{Xe}}(x,y) - I^d(x,y)}. \quad (2)$$

The 2D ratio patterns, $R^e(x,y)$, are converted to one-dimensional (1D) intensity ratio curves, $R^e(s)$, by radial averaging after locating the center position of the diffraction rings; s denotes the momentum transfer parameter which is related to the distance from the center position, as discussed below [see Eq. (4)]. It follows that

$$I^e(s) \cong R^e(s) \times I^t_{\mathrm{Xe}}(s) = I(s) + I^e_B(s), \quad (3)$$

where $I^e_B(s)$ is the sum of $I^a(s)$ and $I^l(s)$. We note that $I^t_{\mathrm{Xe}}(s)$ is the simulated 1D atomic scattering of Xe, and Eq. (3) is valid because the atomic scattering of xenon is much larger than its background gas scattering. Below we shall see how $I^e(s)$ produces the molecular scattering function, which contains all the structural information.

B. Basic theory

The theory of gas-phase electron diffraction is well established and described in the literature (see, for example, Ref. 66). Here, for reference, it will only be briefly summarized. Typically, scattering intensity is expressed in terms of the momentum transfer parameter, s, between the incident and scattered electrons. For elastic scattering, the s value at each pixel point becomes

$$s = |k_0 - k| = 2|k_0|\sin(\theta/2) = \frac{4\pi}{\lambda}\sin(\theta/2), \quad (4)$$

where θ is the scattering angle, $\theta = \arctan(d/L)$, d is the distance from the center position, L is camera distance, and λ is the de Broglie wavelength of the electron. For a given kinetic energy, T, λ becomes

$$\lambda = \frac{hc}{pc} = \frac{hc}{\sqrt{T(T + 2m_0c^2)}}, \quad (5)$$

where h is Planck's constant, m_0 is the rest mass of an electron, and c is the speed of light. With T at 30 keV for an electron experiencing a 30 kV acceleration voltage, λ is 0.069 79 Å. The velocity of the electron at a given kinetic energy is given by

$$v = c\sqrt{1 - \left(\frac{m_0c^2}{T + m_0c^2}\right)^2}. \quad (6)$$

In the independent atomic model, it is assumed that the electronic potential of a molecule is equivalent to an assembly of unperturbed atomic potentials at each appropriate nuclear position within that molecule. Hence, electron scattering from a molecule is simply the sum of each individual atomic contribution and each interatomic molecular interference contribution. The total scattering intensity, $I(s)$, can be written as

$$I(s) = I_A(s) + I_M(s). \quad (7)$$

The atomic scattering, $I_A(s)$, is a sum of elastic and inelastic components for each atom;

$$I_A(s) = \sum_i f_i^2 + 4\frac{S_i}{a_0^2 s^4}, \quad (8)$$

where f_i and S_i are the elastic and the inelastic scattering amplitudes, respectively, for the ith nucleus and a_0 is the bohr radius. Theoretical values of scattering and phase factors are available from the literature.[67] The molecular term, $I_M(s)$, contains the desired structural information and is written for an isotropic distribution of molecules as

$$I_M(s) = \sum_{i,j} f_i f_j \cos(\eta_i - \eta_j)\left\langle \frac{\sin(sr_{ij})}{sr_{ij}} \right\rangle_{\mathrm{vib}}, \quad (9)$$

where η_i is the phase factor for the ith nucleus, r_{ij} is the distance between ith and jth nuclei, and the bracket denotes an average over the vibrational motion. Using the harmonic oscillator approximation, Eq. (9) becomes

$$I_M(s) = \sum_{i,j} f_i f_j \cos(\eta_i - \eta_j)\exp\left(-\frac{1}{2}l_h^2 s^2\right)\frac{\sin(sr_{a,ij})}{sr_{e,ij}}, \quad (10)$$

where $r_{e,ij}$ and $r_{a,ij}$ are the equilibrium and the effective internuclear distances between ith and jth nuclei, respectively, and l_h is the harmonic mean vibrational amplitude. By accounting for the small perturbation by anharmonicity, the effective distance can be expressed by

$$r_a = r_g - \frac{l_h^2}{r_e}, \quad (11)$$

$$r_g = r_e + \tfrac{3}{2}al_h^2, \quad (12)$$

where a is the anharmonicity constant. r_g corresponds to the distance between centers of gravity at temperature T. Often a is set at 2 for direct bonds and at 0 for nonbonded distances. Empirical formulas are used to estimate the harmonic mean vibrational amplitudes, l_h, at room temperature[68] which are then scaled to the experimental temperature.[66]

To visualize the molecular structural parameters as well as emphasize the damped oscillatory behavior, the modified molecular scattering function, $sM(s)$, is defined as

$$sM(s) = s\frac{I_M(s)}{f_I f_J}, \quad (13)$$

where f_I and f_J are atomic scattering factors of the selected nuclei. Sine Fourier transformation then provides the radial distribution, $f(r)$,

$$f(r) = \int_0^{s_{\max}} sM(s)\sin(sr)\exp(-ks^2)ds$$
$$\approx \sum_k sM(s_k)\sin(s_k r)\exp(-ks_k^2)\Delta s_k, \quad (14)$$

which displays the internuclear distance information in an intuitive form. The Gaussian window function $\exp(-ks^2)$ is included to account for the finite range of data acquired. Typically, $k=0.005$ Å^2 for our s range from 2 to 16 Å^{-1}. A piece of the theoretical $sM(s)$ is appended to the low s portion of the experimental $sM(s)$ to provide continuity required by the transform. It is to be noted that for a pair of nuclei i and j, the area under its corresponding peak in the $f(r)$ is proportional to $n_{ij}Z_iZ_j/r_{ij}$ where n_{ij} is the multiplicity of the distance r_{ij} in the molecule. This can be seen from

$$f(r) \propto \sum_{i,j} \frac{Z_iZ_j}{r_{e,ij}\sqrt{2k+l_{ij}^2}} \exp\left[-\frac{(r-r_{a,ij})^2}{2(2k+l_{ij}^2)}\right], \quad (15)$$

where the Gaussian function contains the convolution of both the k damping and l vibrational amplitude (see Refs. 69 and 70). Although the above treatment is for an isotropic distribution, it has been shown elsewhere[71] that orientational effects in UED can be quantitatively expressed.

C. Refining static diffraction data

The experimentally obtained scattering intensity, $I^e(s)$, contains the molecular and atomic scatterings as well as any background, I_B^e, that results from background gas (smoothly varying) and laser scattering (minor), as discussed above. Accordingly,

$$I^e(s) \cong I_M^e(s) + I_A^e(s) + I_B^e(s). \quad (16)$$

From the atomic scattering factors, known in the literature,[67] and the polynomial fit to $I_B^e(s)$, we can obtain the molecular scattering intensity. The experimental modified molecular scattering function becomes

$$sM^e(s) = s\frac{I_M^e(s)}{f_I f_J}, \quad (17)$$

while the theoretical modified molecular scattering function is defined as

$$sM^t(s) = s\frac{I_M^t(s)}{f_I f_J}. \quad (18)$$

Structural refinement is carried out in the modified molecular scattering space by minimizing the difference between the experimental and theoretical $sM(s)$ curves. The difference, χ^2, is defined as

$$\chi^2 = \sum_s \left\{\frac{(sM^e - sM^t)}{\sigma_{sM^e}}\right\}^2, \quad (19)$$

where $\sigma_{sM^e}=s(\sigma_{I^e}/f_I f_J$. It is to be noted that Eq. (19) reduces to

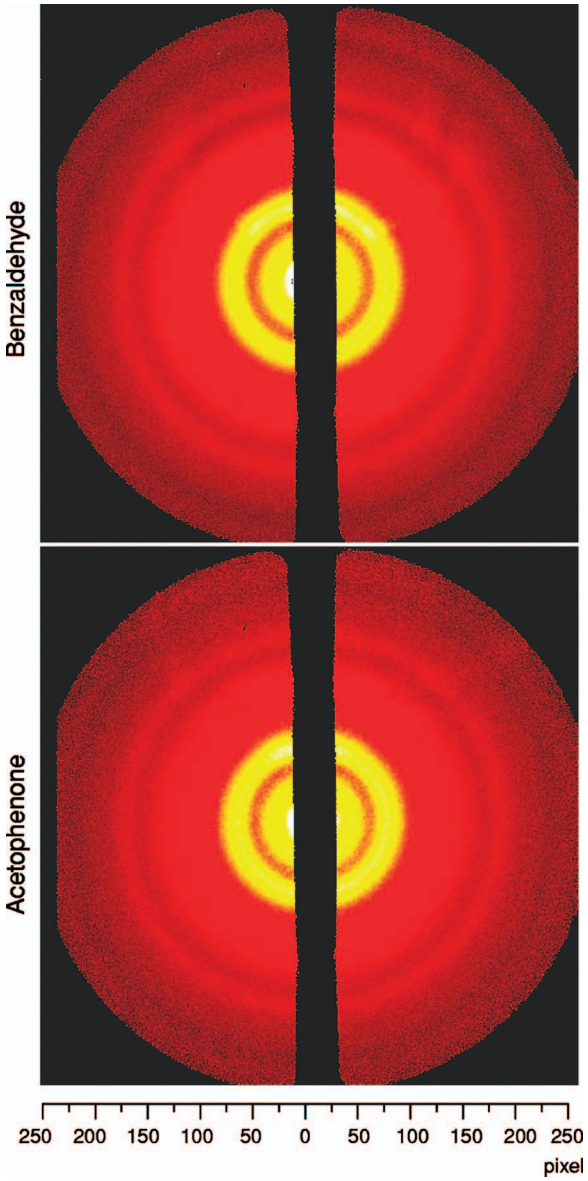

FIG. 5. (Color) Two-dimensional diffraction ratio patterns for benzaldehyde and acetophenone in their ground states.

$$\chi^2 = \sum_s \left\{\frac{I_M^e - I_M^t}{\sigma_{I^e}}\right\}^2 \quad (20)$$

and therefore refinement is unaffected by conversion to $sM(s)$ from the raw intensity space.

The normal equation method (see Ref. 72 and references therein) is employed for linear parameters (scaling factor, polynomial background, and mixture fractions, if any) and the Levenberg-Marquardt algorithm is invoked for nonlinear (structural and vibrational) parameters. χ^2 was primarily used to quantify the fit, although R, a standard goodness-of-fit parameter in electron diffraction, was also checked throughout the refinement.

$$R = \sqrt{\frac{\sum_s \{(sM^e - sM^t)/\sigma_{sM^e}\}^2}{\sum_s (sM^t/\sigma_{sM^e})^2}}. \quad (21)$$

As noted, the difference between χ^2 [Eq. (19)] and R [Eq. (21)] is in the division by the theoretical term of

TABLE III. The refined structures of ground state benzaldehyde and acetophenone.

Molecule	Species	Parameters	Refined value[a]	Theor.[b]
Benzaldehyde[c]	S_0	C1–C2, C6–C1	1.388±0.004	1.401, 1.398
		C2–C3, C5–C6	1.381±0.004	1.388, 1.392
		C3–C4, C4–C5	1.417[d]	1.398, 1.394
		C1–C7	1.480±0.005	1.481
		C7–O8	1.200±0.002	1.209
		C6–C1–C2	120.0±0.7	119.9
		C1–C2–C3, C5–C6–C1	121.0±0.9	119.9, 120.2
		C2–C3–C4, C4–C5–C6	119.1[d]	120.0, 119.7
		C3–C4–C5	119.9[d]	120.3
		C2–C1–C7	120.0[d]	120.3
		C1–C7–O8	126.4±0.3	124.9
		H–C7		1.112
		H–C7–O8		120.7
		H-C_{ring}		1.084–1.086
		H-C_{ring}-C_{ring}		118.5–120.2
		C2–C1–C7–O8		0.0
Acetophenone[c]	S_0	C1–C2, C6–C1	1.407±0.017	1.401, 1.400
		C2–C3, C5–C6	1.401±0.019	1.388, 1.393
		C3–C4, C4–C5	1.380[d]	1.396, 1.393
		C1–C7	1.488±0.034	1.502
		C7–O8	1.198±0.003	1.215
		C7–C9	1.548±0.016	1.519
		C6–C1–C2	118.7±1.4	119.1
		C1–C2–C3, C5–C6–C1	120.0±1.1	120.5, 120.4
		C2–C3–C4, C4–C5–C6	120.7[d]	120.0, 120.0
		C3–C4–C5	120.0[d]	120.0
		C2–C1–C7	120.5[d]	118.1
		C1–C7–O8	124.1±0.4	120.6
		C1–C7–C9	116.0±0.4	118.8
		H-C_{ring}		1.083–1.084
		H-C_{ring}-C_{ring}		120.0–120.1
		H–C9		1.089–1.094
		H–C9–C7		108.5–111.0
		H–C9–C7–O8	29.5±3.0	0.0
		C2–C1–C7–O8		0.0

[a]The error bars reported here are 3σ.
[b]Theoretical structures were obtained at B3LYP/6-311G(d,p) for the ground state of benzaldehyde and acetophenone.
[c]C_{2v} symmetry was imposed for the phenyl ring.
[d]Dependent variables.

$\Sigma_s(sM^t/\sigma_{sM^e})^2$, making R a relative quality of fit parameter. Typically in the analyses we minimize χ^2 and the smaller the R value, the better the agreement; for ground state structural analyses R is typically <0.05, very similar to conventional gas-phase electron diffraction (GED), while for transient structures R is significantly larger.

D. UED diffraction frame reference

Upon irradiation of the molecular beam by the excitation laser, a fraction of the molecules will absorb and undergo photophysical and/or photochemical processes, while most do not interact with the photons and will remain in their initial state throughout the experiment. Molecules absorbing a photon will undergo an electronic transition and possibly structural changes. With this in mind, the scattering intensity at a given time point, t, can be expressed as a sum of scattering intensities for all possible configurations, α.

$$I(s;t) = \sum_{\alpha} I_{\alpha}(s;t) = \sum_{\alpha} f_{\alpha}(t) I_{\alpha}(s), \tag{22}$$

where $f_\alpha(t)$ is the fractional contribution of $I_\alpha(s)$ at time t. This total intensity has a significant component of unreacted, unperturbed molecules in their initial states.

The reacting molecules can be highlighted using the *frame-referencing* method. Diffraction data from before excitation (reference data) are subtracted from diffraction data at time t after excitation. The frame-difference data eliminate essentially all unreacted species as well as the atomic scattering and systematic background, thereby emphasizing the structural changes (and temporal evolution of those structures) during the reaction. For example, for $t_{ref}<0$,

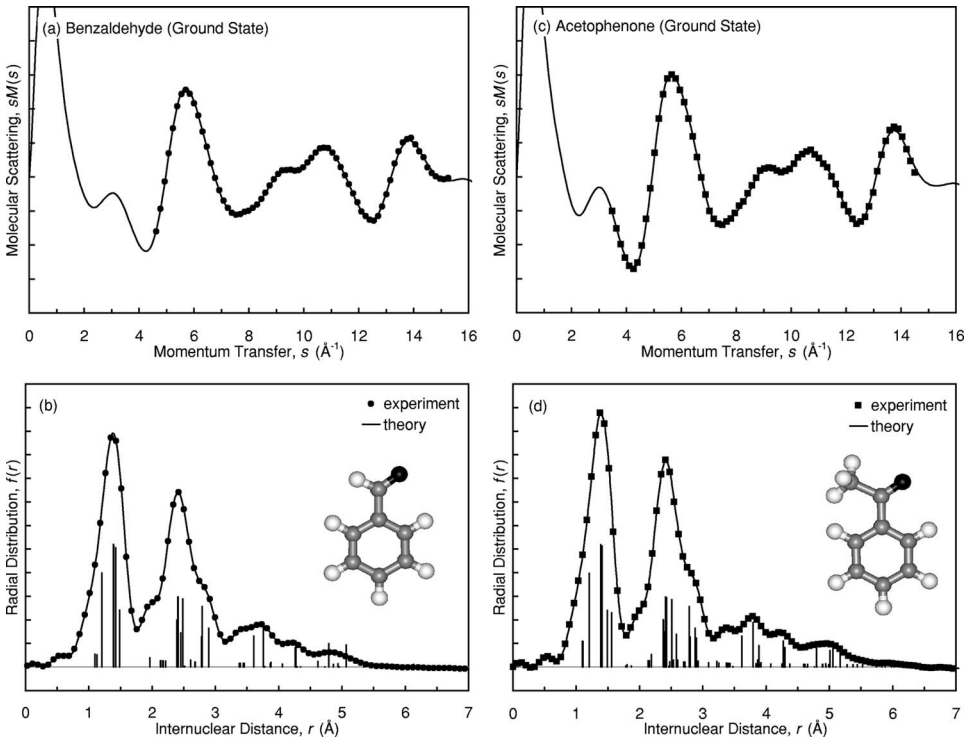

FIG. 6. Modified molecular scattering curves, $sM(s)$, and radial distributions, $f(r)$, for ground state benzaldehyde and acetophenone. The experimental (filled symbols) and theoretical (solid line) of benzaldehyde [(a) and (b)] $R=0.031$ and acetophenone [(c) and (d)] $R=0.028$ in their ground states, together with the refined molecular structures.

$$\begin{aligned}\Delta I(s;t) &= I(s;t) - I(s;t_{\mathrm{ref}}) \\ &= \sum_{\alpha} f_{\alpha}(t) I_{\alpha}(s) - 1 \times I_r(s) \\ &= \left[f_r(t) I_r(s) + \sum_{\alpha \neq r} \{ f_{\alpha}(t) I_{\alpha}(s) \} \right] \\ &\quad - \left\{ f_r(t) + \sum_{\alpha \neq r} f_{\alpha}(t) \right\} I_r(s) \\ &= \sum_{\alpha \neq r} \{ f_{\alpha}(t) I_{\alpha}(s) \} - \left\{ \sum_{\alpha \neq r} f_{\alpha}(t) \right\} I_r(s) \\ &= \sum_{\alpha \neq r} f_{\alpha}(t) \{ I_{\alpha}(s) - I_r(s) \}, \end{aligned} \tag{23}$$

where the r subscript refers to the reference. In this case, because the structure of the reference (ground state) has already been determined, Eq. (23) provides the structures of the intermediates/products and their fractions. $\Delta sM^e(s;t)$ can then be calculated in the same fashion as $sM^e(s)$ was above. The fractional and structural refinements of products and intermediates are carried out with the same nonlinear fitting; minimizing χ^2 in Eq. (19) with $\Delta sM^e(s;t)$ being substituted for $sM^e(s)$ at each time point. A positive time point could also be used as the reference frame in order to enhance the signal of a particular transient structure, as shown elsewhere.[55]

E. Structural refinement and assessment of errors

For each datum, we typically collect 100 diffraction patterns that each consist of 240 000 electron pulse shots (see Sec. III E). These are then averaged to obtain the averaged raw diffraction patterns, $\bar{F}^e$ (sample), $\bar{F}^d$ (detector background), and $\bar{F}^e_{\mathrm{Xe}}$ (xenon). The experimental ratio pattern, $\bar{R}^e$, is then generated with Eq. (2) using these averaged patterns. The error for each pixel of the averaged patterns is then discarded. The 2D ratio patterns, $\bar{R}^e(x,y)$, are converted into 1D intensity ratio curves, $\bar{R}^e(s)$, by radial average. The error in the radial averaging is evaluated by "the standard deviation of the mean" as follows:[73]

$$\sigma_{\bar{R}^e}(s) = \frac{\sqrt{\sum_{r(x,y)=d} \{ \bar{R}^e(x,y) - \bar{R}^e(s) \}^2}}{n_r}, \tag{24}$$

where n_r is the number of pixels in the 2D pattern at a given distance, d, from the center. The experimental error is evaluated by $\sigma_{I^e}(s) = \sigma_{\bar{R}^e}(s) \times I^t_{\mathrm{Xe}}(s)$. During the refinement, the derivative of χ^2 with respect to each parameter φ is utilized to find a minimum position.

$$\beta \equiv -\frac{1}{2} \frac{\partial \chi^2}{\partial \varphi} = 0. \tag{25}$$

The estimated covariance matrix of the standard errors in the fitted parameters becomes

$$[C] \equiv [\alpha]^{-1} = \left[\frac{1}{2} \frac{\partial^2 (\chi^2)}{\partial \varphi_i \partial \varphi_j} \right]^{-1}, \tag{26}$$

from which the variance associated with the estimated parameter φ_i is $\sigma^2(\varphi_i)$ and equals C_{ii}. The error associated with the estimated parameter is

$$\delta(\varphi_i) = \sqrt{\Delta \chi^2_{\nu}} \sqrt{\sigma^2(\varphi_i)}, \tag{27}$$

where $\Delta \chi^2_{\nu}$ is a coefficient determined from the confidence level and the degrees of freedom of the fit, ν; for a table of $\Delta \chi^2_{\nu}$ see Ref. 72.

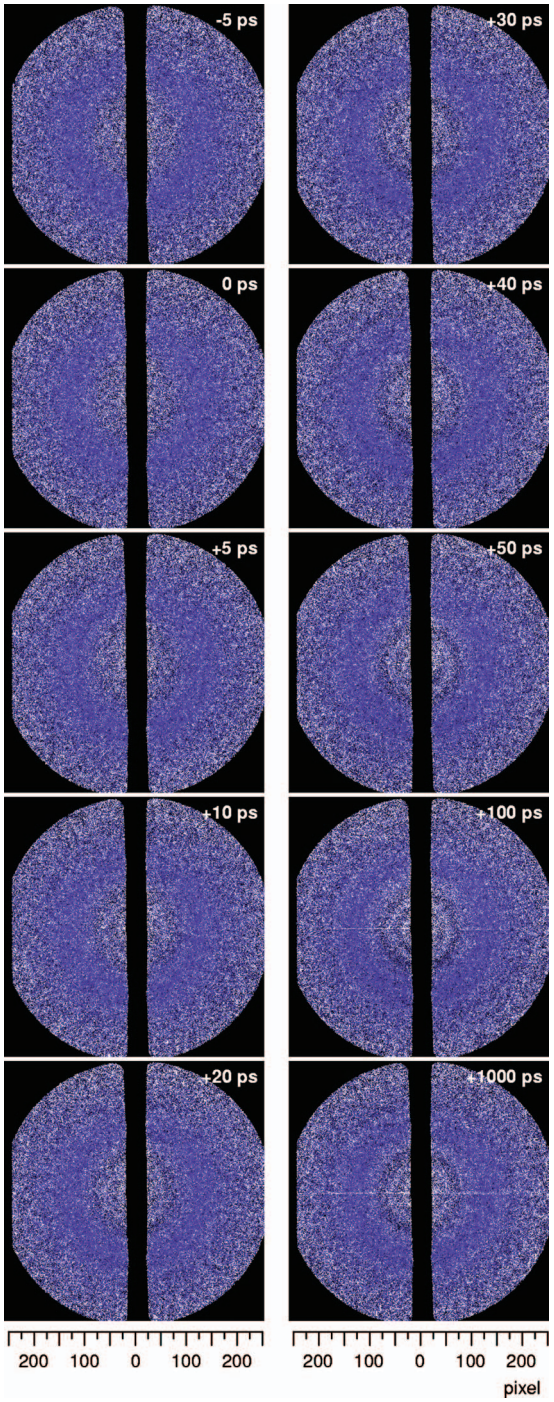

FIG. 7. (Color) Frame-referenced patterns for time-resolved benzaldehyde structural dynamics. The reference frame is at $t=-100$ ps, before the arrival of the excitation laser pulse.

VI. RESULTS

For all results presented, the camera distance was measured independently by recording electron diffraction data from carbon dioxide. Since the molecular structure of carbon dioxide is well known from the literature,[74] the camera distance could be accurately established. For the studies presented here, the camera distances were determined to be 13.38 cm (benzaldehyde studies) and 13.42 cm (acetophenone studies).

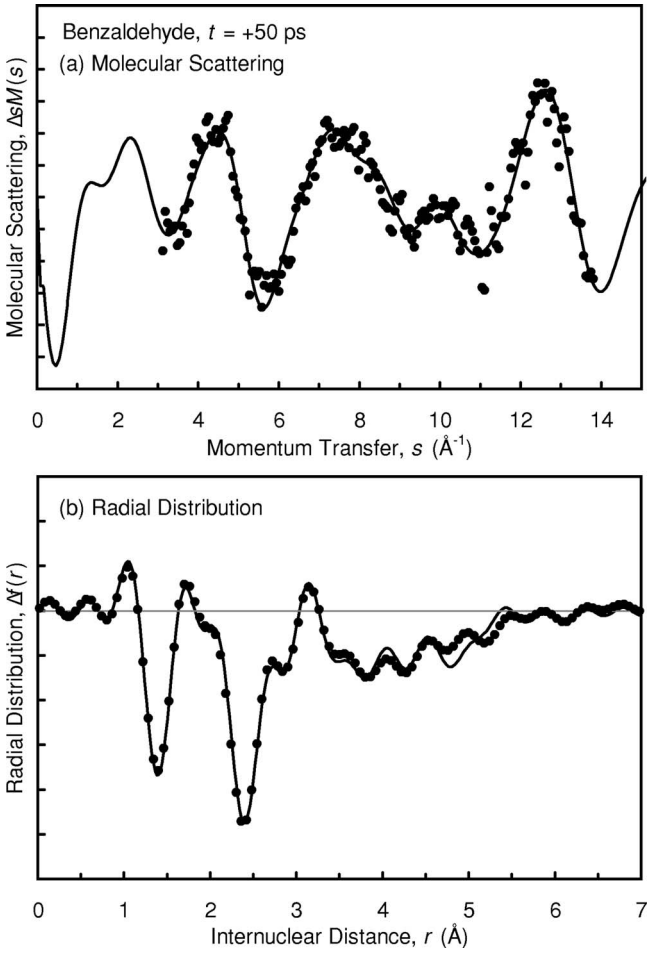

FIG. 8. Modified molecular scattering curves, $\Delta sM(s;t)$, and difference radial distributions, $\Delta f(r;t)$ for benzaldehyde at $t=+50$ ps upon 266.7 nm excitation. The experimental data points are shown as filled symbols and the refined theory is a solid line. ($R=0.399$).

A. Ground state structures: Benzaldehyde and acetophenone

For benzaldehyde, the two-dimensional *ratio* pattern of the ground state diffraction is shown in Fig. 5. Raw data were converted to $sM(s)$ format and compared with the initial guess structure derived from the DFT calculations. The resulting R value is 0.043. The mean amplitudes of vibration were obtained from empirical formulas[68] and extrapolated to 483 K using the nozzle temperature as the temperature of the sample. The polynomial background and theory scaling factor were optimized for the best fit. The data range used for refinement was $s=4.7-15.4$ Å^{-1}, the center of the detector's range.

The structure of benzaldehyde was subsequently refined. As described by Borisenko *et al.* in a previous electron diffraction experiment on benzaldehyde,[33] a C_{2v} model was used for the aryl ring to simplify the refinement; our DFT calculation predicts that the ring is nearly of C_{2v} symmetry. The refined ground state benzaldehyde structural parameters ($R=0.031$) are listed in Table III. Refined bond distances and angles are within 0.01 Å and 1°, respectively, of the structure derived by Borisenko *et al.* The carbonyl torsional angle was tested in preliminary fitting and found to remain nearly planar. For the final refinement, it was fixed in the plane of the

TABLE IV. The refined structures of physical and chemical products.

Molecule	Species	Parameters	Refined value[a]	Theor.[b]
Benzaldehyde	Carbon monoxide	C–O		1.127
	Benzene	C–C	1.371±0.004	1.393
		C–H		1.084
		C–C–C		120.0
		H–C–C		120.0
	Quinoid triplet[c]	C1–C2, C6–C1	1.479±0.029	1.482, 1.474
		C2–C3, C5–C6	1.322±0.029	1.362, 1.358
		C3–C4, C4–C5	1.487[d]	1.442, 1.460
		C1–C7	1.420±0.045	1.421
		C7–O8	1.263±0.031	1.237
		C6–C1–C2	115.6±6.2	117.8
		C1–C2–C3, C5–C6–C1	122.3±7.7	120.3, 120.7
		C2–C3–C4, C4–C5–C6	122.4[d]	121.2, 120.8
		C3–C4–C5	115.0[d]	119.2
		C2–C1–C7	122.2[d]	120.9
		C1–C7–O8	125.4±2.6	123.1
		C7–H		1.087
		H–C7–O8		119.2
		H-C_{ring}		1.072–1.075
		H-C_{ring}-C_{ring}		117.9–120.3
		C2–C1–C7–O8		0.0
Acetophenone	Methyl	C–H		1.080
		H–C–H		120.0
	Benzoyl	C1–C2, C6–C1	1.403±0.024	1.403, 1.398
		C2–C3, C5–C6	1.392[d]	1.388, 1.391
		C3–C4, C4–C5	1.370[d]	1.397, 1.394
		C1–C7	1.487±0.032	1.482
		C7–O8	1.164±0.009	1.186
		C6–C1–C2	120.6±1.1	120.2
		C1–C2–C3, C5–C6–C1	120.1[d]	119.7, 119.9
		C2–C3–C4, C4–C5–C6	116.2[d]	119.9, 119.8
		C3–C4–C5	127.0[d]	120.5
		C2–C1–C7	119.7[d]	120.5
		C1–C7–O8	130.6±2.7	128.5
		H-C_{ring}	1.084	1.084
	Quinoid triplet[c]	C1–C2, C6–C1	1.495±0.014	1.487, 1.474
		C2–C3, C5–C6	1.349±0.021	1.358, 1.356
		C3–C4, C4–C5	1.441[d]	1.446, 1.462
		C1–C7	1.460[d]	1.446
		C7–O8	1.214±0.018	1.224
		C7–C9	1.530[d]	1.516
		C6–C1–C2	117.3±1.3	117.4
		C1–C2–C3, C5–C6–C1	120.7[d]	120.7, 120.8
		C2–C3–C4, C4–C5–C6	119.7[d]	121.1, 121.1
		C3–C4–C5	121.9[d]	118.8
		C2–C1–C7	121.3[d]	119.2
		C1–C7–O8	126.0±7.9	119.8
		C1–C7–C9	117.0[d]	120.4
		H-C_{ring}		1.071–1.075
		H-C_{ring}-C_{ring}		117.6–120.9
		C2–C1–C7–O8	0.8±256	0.0

[a]The error bars reported here are 3σ.
[b]Theoretical structures were obtained at B3LYP/6-311G(d,p) for benzene, carbon monoxide, methyl, and benzoyl. CASSCF(9,10)/6-31G(d) was used for the excited state (T_2) of benzaldehyde, and CASSCF(9,10)/6-311G(d,p) for the excited state (T_2) of acetophenone.
[c]C_{2v} symmetry was imposed for the phenyl ring.
[d]Dependent variables.

ring. In addition, bond distances and angles involving hydrogen atoms were fixed at values given by DFT.

For acetophenone, the molecular structure has been determined for the first time by UED.[2] The combination of a high boiling point and reactivity in the apparatus made working with acetophenone a challenge. Moreover, the molecule, in principle, has numerous similar structural parameters which make the analysis nontrivial. The ratio pattern derived from the raw diffraction pattern is shown in Fig. 5.

The initial guess for the structural refinement was taken from the result of a DFT calculation at B3LYP/6-311G(d,p). As with benzaldehyde, the mean amplitudes of

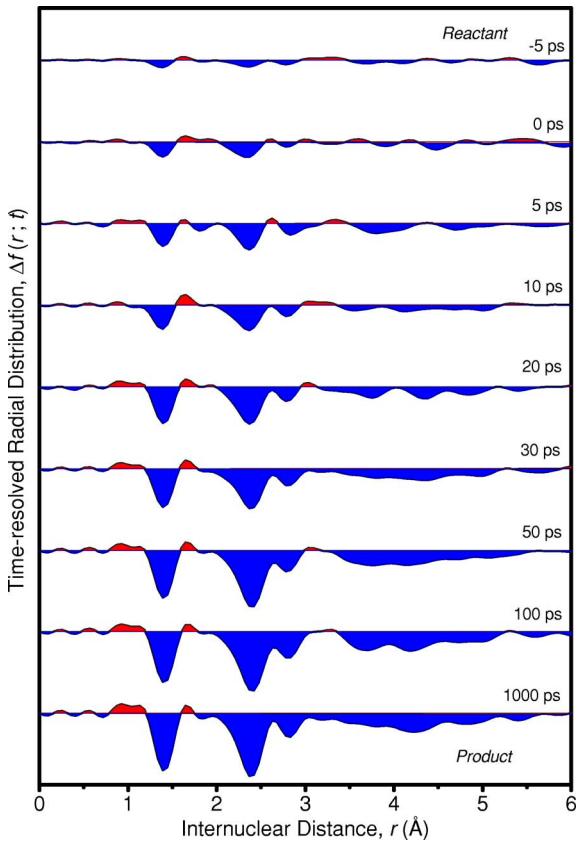

FIG. 9. The experimental $\Delta f(r;t)$ for the photoinduced reaction of benzaldehyde at all time points. Note the rise and eventual leveling off of the difference signal.

vibration were obtained from empirical formulas[68] and extrapolated to 483 K using the nozzle temperature as the temperature of the sample. The polynomial background and theory scaling factor were optimized for the best fit. The data range used for refinement was $s=3.5-14.6$ Å^{-1}.

In order to simplify the refinement process, a C_{2v} symmetry was imposed for the aryl ring; however, the acetyl group was permitted unhindered rotation. The refined structural parameters of ground state acetophenone ($R=0.028$) are listed in Table III. Bond lengths and angles agree with the theoretical values (from DFT) within 0.02 Å and 2°, respectively. A relatively large discrepancy with DFT values was seen in the refined parameters related to the carbonyl and methyl groups: −0.017 and +0.029 Å for the C═O and C–CH_3 distances, respectively, and +3.5° and −2.8° for the carbonyl and methyl angles with respect to the aryl skeleton. The orientation of the methyl hydrogen atoms is observed to deviate from the planar symmetric starting condition, reflecting the freedom of its torsional motion.

The data, $sM(s)$ and $f(r)$, are shown with the refined theoretical models in Fig. 6 for both benzaldehyde and acetophenone.

B. Time-resolved structures: Benzaldehyde

Figure 7 shows the two-dimensional *frame-referenced* patterns for benzaldehyde at 483 K obtained by subtracting the −100 ps ratio pattern from the ratio patterns of the other time points (see Sec. V D). The appearance of diffraction rings in the patterns signifies a structural change between the parent structure (at −100 ps) and the structures formed as a result of the excitation pulse at time zero. The increase in magnitude of structural change with time is readily seen in the time-dependent data (Fig. 7). The same features are retained over time, but only increase in amplitude, signifying the growth in population of a common product structure throughout. The difference data point at +50 ps was selected for the refinement of the theoretical model on the basis of signal quality. The data from $s=3.1-13.9$ Å^{-1} were used, also owing to superior signal quality.

Calculations were performed to arrive at suitable starting geometries for structural refinement (see Sec. IV). Such trial models were based on the various molecules proposed in the literature as products of benzaldehyde photochemistry and the geometries of relevant excited states (see Sec. II). The actual products of photoexcitation were determined by comparing the +50 ps difference data with the theoretical models. Single product reaction models were compared with the data. The models that produce the lowest R values are then used as the initial geometries for structural refinement. For benzaldehyde, the best product fits were the models corresponding to vibrationally "hot" ground state benzaldehyde ($R=0.668$), benzene and carbon monoxide ($R=0.778$), benzene triplet (quinoid and antiquinoid structures) and carbon monoxide ($R=0.448$), and benzoyl radical and atomic hydrogen ($R=0.840$). Structural refinement was attempted with each of these models individually, and in each case the result was an unphysical structure—two long bond distances (>1.6 Å) in the aryl ring. It was concluded that these models individually were each too near to undesired local minima and that a combination of them must be used to account for some more complicated photoreaction. Two-component model comparisons were then performed. Structural refinements were conducted with each dual model, and again, in each case two long bond distances occurred in the aryl rings, except in the cases where T_2 ($^*\pi\pi^*$) benzaldehyde is paired with either benzene and carbon monoxide or the phenyl and formyl radicals. Based on a better χ^2 and previous experi-

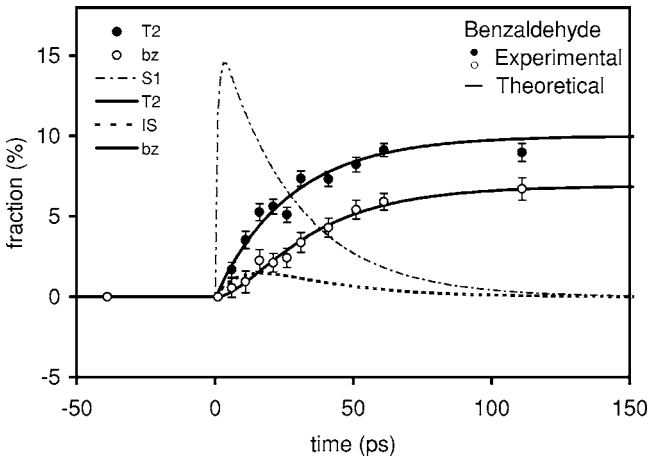

FIG. 10. The time-dependent relative fractions of the each of the benzaldehyde products, T_2 benzaldehyde (solid circles) and benzene + carbon monoxide (open circles). The physical and chemical products are fitted with a kinetic model yielding time constants of 42 and 61 ps, respectively. The time-dependent populations of the other relevant states are also shown.

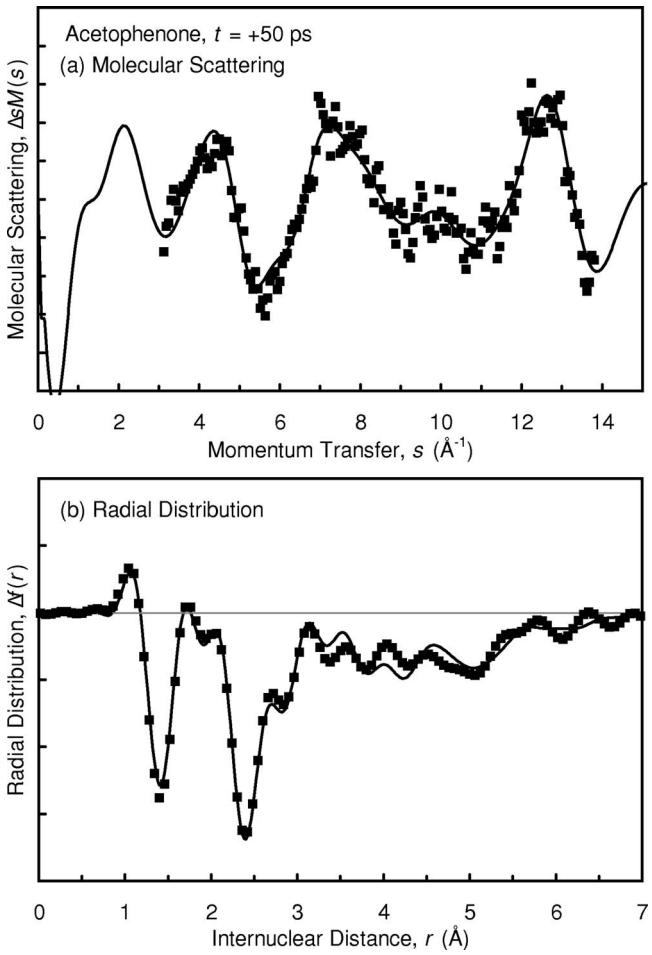

FIG. 11. Modified molecular scattering curves, $\Delta sM(s;t)$, and difference radial distributions, $\Delta f(r;t)$ for acetophenone at $t=+50$ ps upon 266.7 nm excitation. The experimental data points are shown as filled symbols and the refined theory is a solid line. ($R=0.473$).

mental observations of benzene and carbon monoxide as photoproducts,[11,12,35,37–39] the molecular mixture of benzene, carbon monoxide, and triplet $\pi\pi^*$ benzaldehyde were concluded to be the products of this reaction.

The final refined theoretical $sM(s)$ and $f(r)$ are shown with the data in Fig. 8 ($R=0.404$). The structural parameters are listed in Table IV. A C_{2v} model was used for the quinoid benzaldehyde triplet; *ab initio* calculations predict near-C_{2v} symmetry. Since preliminary refinements were rather insensitive to the carbonyl torsional angle, it was fixed at planarity for the final refinement. The structure of ground state benzene was refined with a D_{6h} model. The C≡O distance of carbon monoxide and all structural parameters involving hydrogen atoms were fixed at *ab initio* or DFT-derived values. Contrasting the results of the fit to the theoretically calculated structure shows a few deviations. Most notably, the double bonds of the quinoid ring are somewhat shorter than their theoretical counterparts (1.322/1.322 Å vs 1.362/1.358 Å, respectively) emphasizing the more electron-localized, $\pi\pi^*$ character.

With the final structures now obtained, their contribution at each of the time points is evaluated via linear parameter fitting of the fractions and polynomial background terms. Figure 9 shows time-resolved experimental $\Delta f(r)$ for the refined structures. The experimentally determined population change with time is shown in Fig. 10; relative product fractions at each time point are listed in Table V.

TABLE V. Relative product compositions.

Molecule	Time (ps)	Fraction (%) Photophysical	Photochemical
Benzaldehyde	−100	0	0
	−50	0	0
	−10	0	0
	−5	1.7±0.5	0.6±0.6
	0	3.5±0.5	0.9±0.7
	5	5.3±0.5	2.3±0.7
	10	5.6±0.5	2.1±0.6
	15	5.1±0.5	2.4±0.6
	20	7.4±0.5	3.4±0.6
	30	7.3±0.5	4.3±0.6
	40	8.2±0.5	5.4±0.6
	50	9.1±0.4	5.9±0.5
	100	9.0±0.6	6.7±0.7
	1000	10.9±0.5	6.7±0.7
Acetophenone	−100	0	0
	50	8.9±0.8	11.9±0.8
	100	8.4±0.8	16.8±0.8

The error bars reported here are 3σ.

Both the photophysical (T_2, $\pi\pi^*$ benzaldehyde) and photochemical (benzene+CO) channel products grow simultaneously. The apparent rise time constant of the channel forming T_2 benzaldehyde is 25±4 ps, determined by nonlinear fitting of a single step reaction. The rise time constant of the benzene-forming channel is somewhat longer, 38±5 ps. The final percent populations of T_2 benzaldehyde and benzene are 10.0% ±0.4% and 6.9% ±0.2%, respectively, after reaching stationary state; the percentage is in reference to the total population of all species [Eq. (22)]. The nearly parallel behavior of the two product channels implies competitive bifurcation after origination from a single state, as no growth of one at the expense of the other was observed. At our excitation, to the $\pi\pi^*$ S_2, it is known that the state has an ultrashort lifetime [~250 fs (Ref. 20)]. Because of this, and the fact that intersystem crossing (ISC) is more efficient between states of different orbital excitations ($\pi\pi^*/n\pi^*$), it follows that T_2 ($\pi\pi^*$) benzaldehyde must form from an $n\pi^*$ state via an efficient ISC, making S_1 benzaldehyde the origin state of bifurcation.

The bifurcation dynamic model of benzaldehyde can now be written as follows:

$$S_0 \xrightarrow{h\nu} S_2 \xrightarrow{k_{IC}} S_1 \begin{cases} \xrightarrow{k_{ISC}} T_2 \\ \xrightarrow{k_i} \mathrm{IS} \xrightarrow{k_d} \mathrm{Bz} + \mathrm{CO} \end{cases} \quad (28)$$

An intermediate structure (IS) is included in order to account for the difference in the rise time of the two channels bifurcated from the hot S_1 $n\pi^*$ state. The presence of the IS is further supported by the electronic nature of S_1—dissociation from the $n\pi^*$ excited state correlates with the electronically excited state of CO which is not seen in the data. It follows

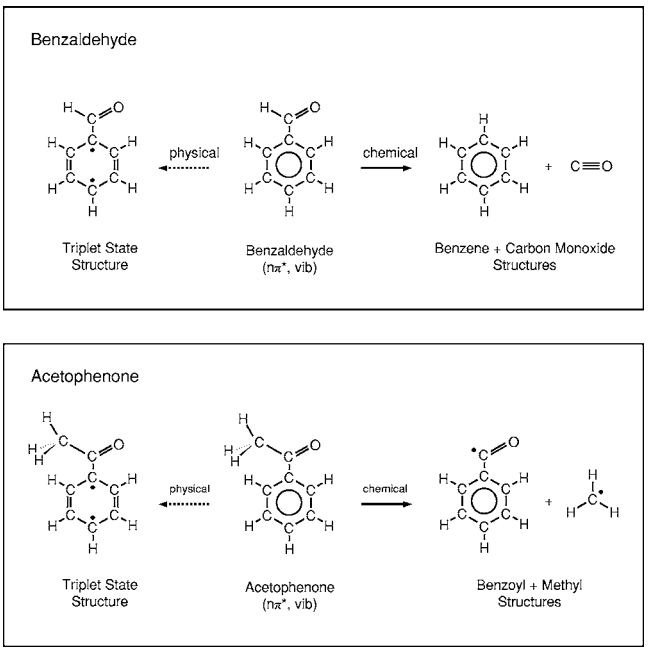

FIG. 12. Structures involved in the photophysical and photochemical processes of benzaldehyde (top) and acetophenone (bottom) on our experimental time scale.

that the total decay rate of the S_1 population is given by

$$k = k_{\mathrm{ISC}} + k_i \tag{29}$$

and the product branching ratio is

$$\frac{P(T_2)}{P(\mathrm{Bz}+\mathrm{CO})} = \frac{k_{\mathrm{ISC}}}{k_i}. \tag{30}$$

From the rise time of 25 ± 4 ps ($k=4.0\times10^{10}\pm0.6\times10^{10}$ s^{-1}) for the faster channel and a branching ratio (T_2:Bz+CO) of $10.0\%\pm0.4\%:6.9\%\pm0.2\%$, the rate constants are found to be $k_{\mathrm{ISC}}=2.4\times10^{10}$ s^{-1} ($1/k_{\mathrm{ISC}}=42$ ps) and $k_i=1.6\times10^{10}$ s^{-1} ($1/k_i=61$ ps). A simulation of the population changes based on this bifurcation model is shown with the data in Fig. 10; k_d was taken to be 9.4×10^{10} s^{-1} ($1/k_d=11$ ps) from the initial rise of the benzene channel. The decay of the S_1 was not seen due to its structural similarity with the parent S_0; the very short-lived IS was not detectable because of its small population (see Fig. 10).

C. Time-resolved structures: Acetophenone

Diffraction data at three time points (−100, +50, and +100 ps) were taken for acetophenone. The full temporal range of experimentation was limited because of inlet window coating mentioned in Sec. III C. The data from −100 ps were used as the reference and subtracted from the positive time points to generate the difference data. Perusal of both patterns and curves reveals a signal that is nearly, but not entirely, saturated 50 ps after the excitation laser pulse. Product analysis was conducted on both time points and found to yield equivalent results. The results presented hereafter were arrived at through analysis of the +50 ps difference data, unless otherwise noted.

Determination of the products of acetophenone photolysis was performed similar to that described previously for benzaldehyde. First, structures proposed in the literature and our own calculations were compared with the difference data. Products used in these comparisons have been speculated by previous photochemical and photophysical works. The best single product fit, by R value, is the channel leading to toluene and carbon monoxide as products ($R=0.636$). Attempts at structural refinement of the single products produced geometries that were unphysical (direct bond distances >1.6 Å). The best dual product fit is the product combination of T_2 ($\pi\pi^*$) acetophenone, toluene, and carbon monoxide ($R=0.584$).

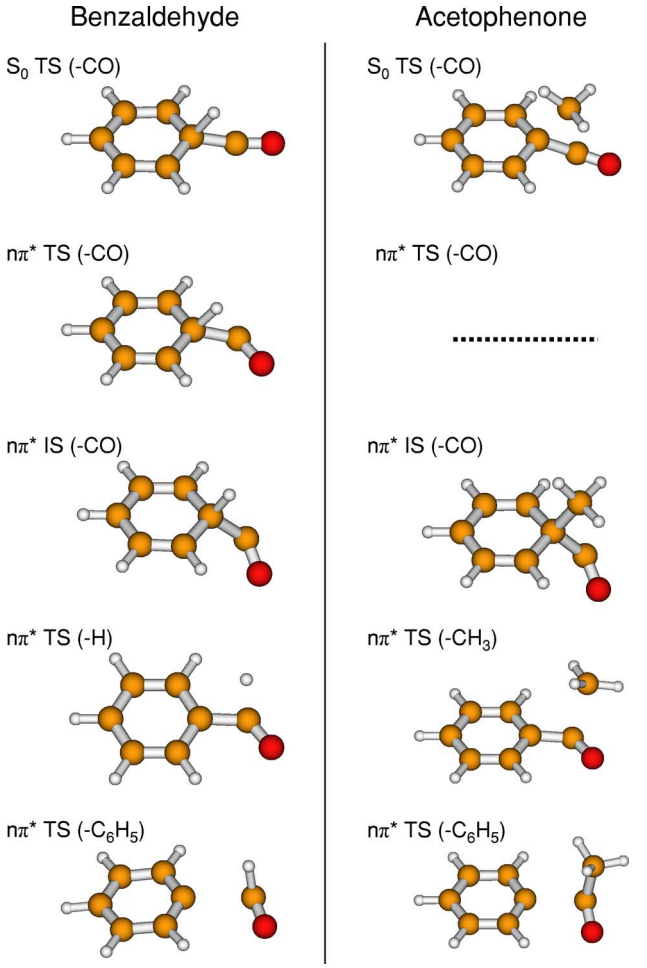

FIG. 13. The geometries of transition states and intermediates in the reactions of benzaldehyde (left) and acetophenone (right). Calculations were performed at the B3LYP/6-311G(d,p) level and include pathways observed and some that represent other possibilities.

Continuing to follow the procedure used for analyzing the benzaldehyde data, structural refinement was also performed on several of the dual product models. The molecular dissociation pathway which had worked well for benzaldehyde was not compatible with the acetophenone data despite the favorable *ab initio* comparison. Refinement of that model caused the contribution of T_2 acetophenone to be eliminated entirely leaving only toluene and carbon monoxide. The structure of toluene was also changed significantly; two of the C–C bonds of the aryl ring stretched to 1.57 Å and the methyl group became separated from the ring by 1.98 Å. The improbable geometry excluded this product channel from

TABLE VI. Statistical and mode-limited rate constants.

Molecule	Channel		Energy[a,b] (cm^{-1}) Reactant	TS	IS	Product	Rate[c,d] (s^{-1}) k_6	k_n	k_s
Benzaldehyde	S_0	–CO	0	*32 218*	···	460	1.7×10^{10}	2.1×10^{8}	5.4×10^{0}
		–H	0	···	···	*32 679*			
		$-C_6H_5$	0	···	···	34 611			
	S_1	–CO	26 921	*35 474*	*28 439*	30 087	1.6×10^{11}	1.3×10^{10}	1.0×10^{7}
		–H	26 921	*36 297*	···	*32 682*	7.7×10^{10}	5.6×10^{9}	6.6×10^{6}
		$-C_6H_5$	26 921	*36 772*	···	*34 611*	5.0×10^{10}	3.9×10^{9}	1.6×10^{7}
Acetophenone	S_0	–CO	0	*33 697*	···	1 816	6.2×10^{9}	1.4×10^{5}	8.0×10^{-3}
		$-CH_3$	0	···	···	*29 751*			
		$-C_6H_5$	0	···	···	*34 291*			
	S_1	–CO	27 279	×	*29 810*	30 890			
		$-CH_3$	27 279	*34 257*	···	*29 751*	6.7×10^{11}	1.6×10^{10}	3.5×10^{8}
		$-C_6H_5$	27 279	*36 951*	···	34 291	3.5×10^{10}	2.1×10^{8}	2.9×10^{6}

[a]The energy corrections for S_1 ($^1n\pi^*$) reactions are 3906 and 3710 cm^{-1} for benzaldehyde and acetophenone, respectively (see text).
[b]The energy corrections for products are 2276 cm^{-1} for C_6H_5CO+H and 3091 cm^{-1} for $C_6H_5CO+CH_3$.
[c]k_6, k_n, and k_s denote statistical rate constants for various models of energy coupling among phenyl, methyl, and carbonyl groups. k_6 (for six involved modes) is obtained by assuming that the phenyl and methyl groups do not participate in energy randomization (spectator model), and k_s by assuming full randomization of reactant energy amongst all vibrational modes. k_n is obtained by assuming partial randomization where only n vibrational modes participate in the dissociation; $n=10$ for benzaldehyde and $n=16$ for acetophenone are used.
[d]Thermal energies at 500 K were added to the excitation energy of 37 500 cm^{-1} (266.7 nm).

further consideration. Structural refinement of several other two-product models resulted in similar behavior.

Well-behaved structural refinement was found with the model corresponding to the channels forming T_2 acetophenone and the benzoyl and methyl radicals. The final refined theoretical model is shown with the data in Fig. 11. The fitted structural parameters are listed in Table IV along with those predicted by theory. In this refinement it was necessary to employ structural dependencies to simplify the fitting. In addition to the restriction of C_{2v} symmetry for the aryl rings in both benzoyl radical and T_2 acetophenone, the models of both molecules were further restricted. Only one distance and one angle were refined in the ring of the benzoyl radical and, for T_2 acetophenone, all single bonds were defined by one "fittable" parameter. Furthermore, the skeletal angles of the T_2 acetophenone ring were defined as one, as were the angles of the carbonyl moiety. And, as is typical of all ring structures, some parameters were unable to be defined and simply drifted with the changes of the other, fittable parameters. The torsional angles for carbonyl groups in the benzoyl radical and in T_2 acetophenone were fixed in the plane of the ring, as indicated by theory and preliminary fitting results. Differences between the parameters derived from the diffraction data and those calculated by theory were less than 0.03 Å for bond distances and 3° for angles, or were within the error bar. The double and single bonds of the T_2 acetophenone ring are clearly resolved demonstrating the loss of aromaticity and its $\pi\pi^*$ nature.

Upon the acquisition of the structures of the reaction products, their fractional contributions were obtained at the +100 ps difference time point (recall that structural refinement was conducted at the +50 ps difference time point). From +50 to +100 ps the fractional amount of T_2 acetophenone remains unchanged, but the amount of fragmentation into benzoyl and methyl radicals increases over the two time points from $11.9\%\pm0.8\%$ at +50 ps to $16.8\%\pm0.8\%$ at +100 ps. This is a similar case to that reported above for benzaldehyde where dissociation also occurs at a slower rate. Because of the limited data points we cannot elucidate the exact nature of the bifurcation. However, the structures determined lead us, in analogy with benzaldehyde, to the following mechanism:

$$S_0 \xrightarrow{h\nu} S_2 \xrightarrow{k_{IC}} S_1 \begin{cases} \xrightarrow{k_{ISC}} T_2 \\ \xrightarrow{k_d} C_6H_5CO + CH_3. \end{cases} \tag{31}$$

The relative fractions of the products are listed in Table V. The observed structures involved in the photophysical and photochemical bifurcations in both benzaldehyde and acetophenone are shown in Fig. 12.

VII. DISCUSSION

The results of our UED studies of benzaldehyde and acetophenone can be summarized as follows. The ground state structures of benzaldehyde and acetophenone were determined. The structural parameters refined for the benzaldehyde data agree well with previous conventional electron diffraction results.[33] To our knowledge, the molecular structure of acetophenone has not been determined previously. For both systems, it was possible to study the structural dynamics following ultrafast laser excitation at 266.7 nm to the S_2 ($\pi\pi^*$) excited state. The photophysical and photochemical channels were observed in competition and the resultant molecular structures characterized. Time scales were also determined.

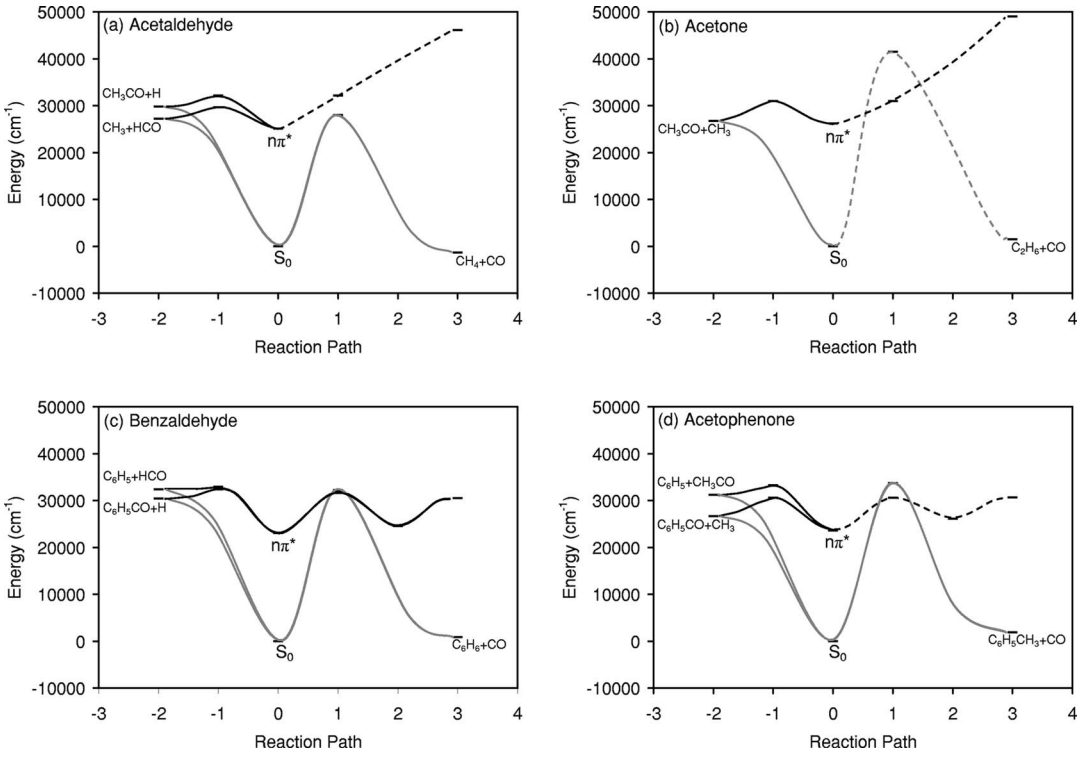

FIG. 14. Calculated reaction coordinates of radical cleavage and molecular dissociation pathways of (a) acetaldehyde, (b) acetone, (c) benzaldehyde, and (d) acetophenone on the ground electronic surface and the T_1, $n\pi^*$ surface. Calculations were performed at the B3LYP/6-311G(d,p) level.

The refinement of the structures present in the time-resolved diffraction data for acetophenone and benzaldehyde results from the bifurcation on the excited S_1 $n\pi^*$ state, following femtosecond internal conversion from S_2, which results in the formation of a quinoid triplet structure and the products of dissociation. For benzaldehyde the dissociation products are the closed-shell molecular species, benzene and carbon monoxide. For acetophenone they are the benzoyl and methyl radicals.

It is to be noted that UED is uniquely suited for elucidating such excited state behavior. The T_2 states of these molecules are "dark" and have eluded spectroscopic studies for decades. UED does not rely on brightness and instead reveals information regarding every structure present in the interaction region at any given time.

A. Structural dynamics

Given the UED results above, the following dynamical picture of aromatic carbonyl photophysics and photochemistry can be drawn. Excitation at 266.7 nm promotes population of both acetophenone and benzaldehyde into the $\pi\pi^*$ S_2 state which decays rapidly by internal conversion into S_1. For benzaldehyde at our excitation, the decay time is roughly 250 fs and for acetophenone S_2 lives less than 140 fs.[20] In the nascent vibrational levels of S_1, aromatic carbonyl molecules experience a bifurcation of pathways. A physical pathway moves some population into the triplet manifold, the $\pi\pi^*$ T_2 state, and a competitive chemical pathway causes dissociation into products.

For benzaldehyde, the physical channel (ISC) from S_1 proceeds with a rate of 2.4×10^{10} s^{-1} ($1/k_{\mathrm{ISC}}$=42 ps) and survives up to at least 1 ns; the measured rate is $k_{\mathrm{ISC}}+k_i$ [see Eq. (29)]. The triplet structure was identified as that of the $\pi\pi^*$ T_2 and, compared to the ground state, the phenyl ring is seen to distort as aromaticity is lost—two double bonds and four single bonds make up the quinoid ring. Along the chemical pathway, the benzene and carbon monoxide products are formed stepwise, involving an IS, as determined by the observed kinetics detailed in Sec. VI B.

After internal conversion to the $n\pi^*$ S_1, excitation is localized mainly on the C=O bond of the carbonyl group. According to our quantum chemical calculations, the carbonyl group remains coplanar with the phenyl ring; however, the H–C=O out-of-plane bending mode is reduced in frequency (642 cm^{-1} on $n\pi^*$ compared with 1033 cm^{-1} on S_0). The more facile large-amplitude motion of the aldehydic hydrogen atom allows for its capture by C1 and the subsequent formation of a transition state (TS) where the H is shared by C1 and C7 (shown in Fig. 13). This TS connects the $n\pi^*$ state to IS where C1 is sp^3 hybridized and bound to both H and CO (also shown in Fig. 13). The aldehydic hydrogen atom and the CO moiety are loosely bound and distorted from the molecular plane and either can be lost from IS by simple cleavage. Pathways are depicted in Fig. 14. Perturbation present in the C=O moiety of the $n\pi^*$ state switches in the intermediate to a $\pi\pi^*$-like perturbation of the phenyl group resulting in a "pseudoprefulvenic" six-membered ring structure. The C=O distance in the intermediate is identical to the C=O distance of the acetyl radical ground state (1.180 Å), indicating the stability of the CO moiety.

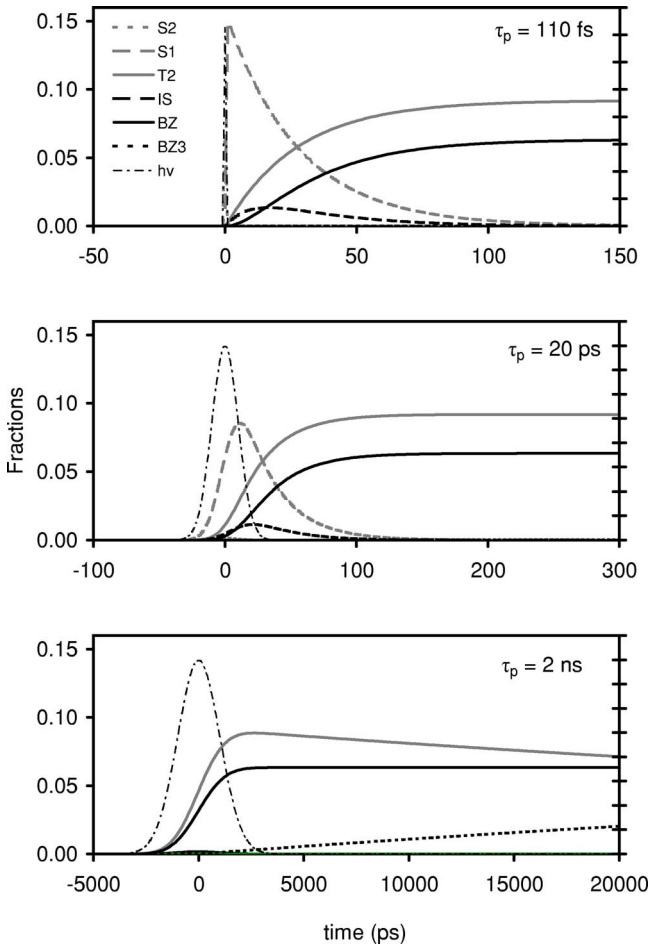

FIG. 15. Dynamical model of population flow of states relevant to the photophysical and photochemical processes of excited benzaldehyde. The panels show the relative component fractions based on laser excitation by a 266.7 nm pulse of (a) 110 fs, (b) 20 ps, or (c) 2 ns duration.

UED results show that the rearrangement step (S_1 to IS) takes place at a rate of 1.6×10^{10} s^{-1} ($1/k_i$=61 ps); the measured rate is $k_{ISC}+k_i$ [see Eq. (29)]. But, statistical Rice-Ramsperger Kassel-Marcus (RRKM)[75] calculations predict a rate several orders of magnitude slower (see Table VI), implying that energy redistribution among vibrational modes may be incomplete. The TS between the $n\pi^*$ state and IS is lower in energy than both the $n\pi^*$ TS leading to benzoyl and hydrogen radicals as well as an S_0 TS leading directly to benzene and carbon monoxide products. The structures of the various theoretical transition states and intermediates are shown in Fig. 13. Passage from the excited state IS to the products may proceed in different ways. The most direct route would be dissociation of CO from IS. However, an alternative route exists through the ground state—although a frequency calculation confirms the stability of IS in the excited state, it immediately undergoes CO loss when put on the S_0 surface. Internal conversion of IS followed by instantaneous dissociation could be the more likely path. The threshold energy for benzene formation from benzaldehyde is known to be just below the S_2 origin with which the above theoretical estimation agrees quite reasonably.[5,7,12,16] If instead we were to assume that the molecular dissociation occurs after internal conversion from S_1 to S_0, we have calculated that the large barrier height (32 218 cm^{-1}) will render the reaction much slower than the time scale observed (see Table VI).

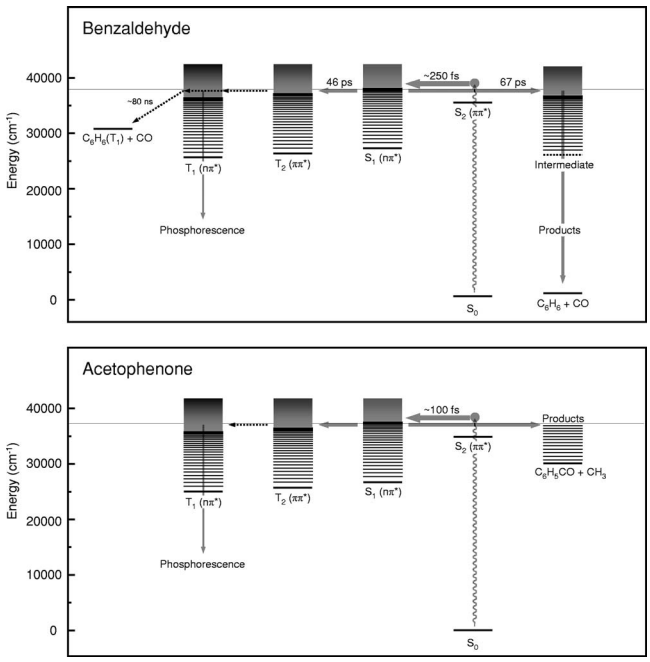

FIG. 16. The bifurcation into photochemical and photophysical processes upon excitation of benzaldehyde (top) and acetophenone (bottom).

For acetophenone, the bifurcation from S_1 is also seen as a competition between chemical and physical pathways. The physical pathway results in the formation of a $\pi\pi^*$ triplet, structurally similar to the quinoid ring seen for benzaldehyde. However, the chemical result is quite different. On the excited state, the methyl group does not show the same propensity for large-amplitude motion as was seen for the aldehydic hydrogen of S_1 benzaldehyde and its capture by the phenyl ring does not occur. In other words, a pathway (or TS) could not be found for the molecular dissociation channel from the $n\pi^*$ state—although an IS such as that found for the benzaldehyde dissociation can be calculated for acetophenone (see Fig. 13), no direct trajectory exists to link it to S_1. Methyl loss is the lowest energy chemical channel found from the $n\pi^*$ surface. The quantum chemical calculations above agree well with our experimental observations; molecular dissociation for benzaldehyde and radical cleavage for acetophenone are the favored chemical pathways from their respective $n\pi^*$ states.

B. Spectroscopic observations revisited

The T_2 states of acetophenone and benzaldehyde are electronic states that have eluded direct characterization by all previous experimental methods. As described in Sec. II, phosphorescence studies have supplied all that is known of the state and its relationship to the bright T_1. Some previous researchers[11,38] employed a kinetic model with an intermediate state in the triplet manifold, with a lifetime long enough to explain the collision-induced quenching of chemistry and the enhancement of phosphorescence in high pressure envi-

ronments. The UED results permit us to identify this reactive, yet quenchable, intermediate as T_2. If T_2 is allowed to evolve in the absence of collisions, dissociation occurs to produce the triplet benzene observed by other researchers on longer time scales.[38,39] The dissociation time constant for this reaction would be about 80 ns at our excitation energy. The triplet state of $\pi\pi^*$ benzene and ground state of CO theoretically correlate as molecular dissociation products of T_2 $\pi\pi^*$ benzaldehyde. If, however, T_2 loses its excess vibrational energy through collisions, the only significant relaxation pathway becomes phosphorescent emission through T_1. In other words, phosphorescence is the dominant process in aromatic carbonyl compounds possessing little excess energy above the S_1 origin. In the isolated molecule, at energies above S_2 excitation the expected yield of benzene and carbon monoxide is nearly unity (phosphorescence is a minor channel).[4,11,37] This unity yield of benzene is actually the sum of two separate benzene-forming reactions: the fast singlet channel and the slow triplet channel.

The steady population of T_2 up to 1 ns delay seen by UED confirms the slowness of a further chemical channel but also signifies the lack of irreversible population transfer to T_1. Since the energy gap between T_2 and T_1 is known to be so small, it may be explained by a mixed state or by rapid and "reversible" internal conversion between the two. However, the structural similarity of T_1 and S_0 precludes the detection of T_1 in this UED study, and confirmation of its presence was not possible.

Benzene formation through the photodissociation of benzaldehyde has previously been the subject of multiphoton ionization (MPI) studies using different pulse widths.[35–37,39] These inquiries have provided a reaction time scale between 20 ps and 2 ns. In order to unite our UED results with these from the literature, simulations of population evolution have been performed following the photophysical and photochemical mechanisms described in Eq. (28) and using the rate constants available. Population changes were calculated by numerical integration of the differential equations of the kinetic model using the fourth order Runge-Kutta method.[72] Multiphoton ionization of neutral species to their ionic counterparts was also included. Laser pulse widths of 110 fs, 20 ps, and 2 ns are used to model each type of experiment (ours and others, see Refs. 35–37). The time-dependent population changes and laser profiles are shown in Fig. 15. Using a 20 ps ultraviolet pulse, the simulation predicts a branching ratio of 94%: 6% for molecular and benzene ion yields, respectively, while one for a 2 ns excitation laser pulse predicts a ratio of 6%: 94%. Both results are in qualitative agreement with the MPI experiments.[35] It should be noted that our simulation is based on the assumption that two-photon absorption cross sections for photoionizations of both excited benzaldehyde and ground state benzene are similar, although in reality they should strongly depend on wavelength, electronic structure, and resonance.

To better understand the differences between the photochemistries of acetophenone and benzaldehyde, it is valuable to compare them with the aliphatic carbonyl molecules, acetone and acetaldehyde (see Fig. 14). Acetaldehyde is a prototypical aldehyde and is known to undergo "*molecular dissociation*" (CO abstraction)[76] as well as "*homolytic cleavage*" (radical fragmentation) upon UV absorption. Acetone, the prototypical ketone, however, undergoes only a homolytic radical cleavage well known as the Norrish type-I reaction.[65,77] A molecular dissociation channel has never been reported. It has been established that the molecular dissociation pathway of acetaldehyde occurs after internal conversion to the hot S_0 while radical channels take place after ISC. Radical cleavage of acetone is also believed to occur after ISC to the triplet manifold; however, it has been recently proposed[65] and confirmed[78] that fragmentation occurs directly from S_1 and yields an electronically excited acetyl radical which then undergoes internal conversion.

Although there are some analogies between aromatic and aliphatic carbonyl compounds, the physics and chemistry of aromatic carbonyl molecules are more complex due to the addition of close-lying $\pi\pi^*$ states to the manifold of low-lying $n\pi^*$ states provided by the carbonyl group. Namely, an $n\pi^*$ state, when located near a $\pi\pi^*$ state, can provide additional pathways for an aromatic carbonyl via energetically stable intermediates. Therefore, benzaldehyde (aromatic) may perform the molecular dissociation reaction through an intermediate structure on the excited state where it is the most energetically favored channel, while acetaldehyde (aliphatic) undergoes molecular dissociation on its ground state. Acetophenone, lacking a mobile hydrogen, may very well fragment following the mechanism of its aliphatic analog, acetone.

VIII. CONCLUSION

Structural dynamics of the aromatic carbonyls benzaldehyde and acetophenone (see Fig. 16) have been studied using the methodology of ultrafast electron diffraction. Following S_2 $(\pi\pi^*)$ excitation at 266.7 nm, a bifurcation of pathways between photophysics (intersystem crossing) and photochemistry (molecular dissociation or radical cleavage) was observed. Intersystem crossing in both molecules results in a "quinoidlike" structure for the excited state, T_2 $(\pi\pi^*)$. The product structures revealed different chemistries for benzaldehyde and acetophenone, elucidating the fundamental disparity between aromatic aldehydes and ketones. Theoretical calculations support that the distinction results from a more facile large-amplitude motion of the aldehydic hydrogen compared to the methyl substituent. The photophysics of these molecules is made clear as UED has allowed for the direct detection and structural characterization of the dark structure of the T_2 state. Furthermore, the relationship between physical and chemical pathways in these molecules has been elucidated and a comprehensive picture of the structure of excited-state landscapes and pathways has been drawn.

ACKNOWLEDGMENTS

We would like to thank the National Science Foundation and the Air Force Office of Scientific Research for providing support for this work. We would also like to thank Dr. Shoujun Xu for his assistance in the design of the sample inlet.

[1] R. Srinivasan, J. S. Feenstra, S. T. Park, S. Xu, and A. H. Zewail, Science **307**, 558 (2005).
[2] J. S. Feenstra, S. T. Park, and A. H. Zewail, J. Chem. Phys. **123**, 221104 (2005).
[3] G. Thiault, A. Mellouki, G. Le Bras, A. Chakir, N. Sokolowski-Gomez, and D. Daumont, J. Photochem. Photobiol., A **162**, 273 (2004).
[4] Y. Hirata and E. C. Lim, J. Chem. Phys. **72**, 5505 (1980).
[5] T. Itoh, Chem. Phys. Lett. **133**, 254 (1987).
[6] M. B. Robin and N. A. Kuebler, J. Am. Chem. Soc. **97**, 4822 (1975).
[7] T. Itoh, H. Baba, and T. Takemura, Bull. Chem. Soc. Jpn. **51**, 2841 (1978).
[8] N. Ohmori, T. Suzuki, and M. Ito, J. Phys. Chem. **92**, 1086 (1988).
[9] E. Villa, A. Amirav, W. Chen, and E. C. Lim, Chem. Phys. Lett. **147**, 43 (1988).
[10] A. Inoue and N. Ebara, Chem. Phys. Lett. **109**, 27 (1984).
[11] M. Berger, I. L. Goldblatt, and C. Steel, J. Am. Chem. Soc. **95**, 1717 (1973).
[12] U. Brühlmann, M. Monella, P. Russegger, and J. R. Huber, Chem. Phys. **81**, 439 (1983).
[13] C. R. Silva and J. P. Reilley, J. Phys. Chem. **100**, 17111 (1996).
[14] M. Biron and P. Longin, Chem. Phys. Lett. **116**, 250 (1985).
[15] T. Itoh, Chem. Phys. Lett. **151**, 166 (1988).
[16] T. Itoh, T. Takemura, and H. Baba, Chem. Phys. Lett. **40**, 481 (1976).
[17] M. Kiritani, T. Yoshii, N. Hirota, and M. Baba, J. Phys. Chem. **98**, 11265 (1994).
[18] M. Koyanagi and L. Goodman, Chem. Phys. **39**, 237 (1979).
[19] O. Sneh and O. Cheshnovsky, J. Phys. Chem. **95**, 7154 (1991).
[20] S.-H. Lee, K.-C. Tang, I.-C. Chen, M. Schmitt, J. P. Shaffer, T. Schultz, J. G. Underwood, M. Z. Zgierski, and A. Stolow, J. Phys. Chem. A **106**, 8979 (2002).
[21] Y. Kanda, H. Kaseda, and T. Matamura, Spectrochim. Acta **20**, 1387 (1964).
[22] H. Murai and K. Obi, J. Phys. Chem. **79**, 2446 (1975).
[23] S. Nagaoka and N. Hirota, Bull. Chem. Soc. Jpn. **56**, 3381 (1983); L. Goodman and M. Koyanagi, Mol. Photochem. **4**, 369 (1972).
[24] I. Ozkan and L. Goodman, Chem. Phys. Lett. **64**, 32 (1979).
[25] H. Hayashi and S. Nagakura, Mol. Phys. **27**, 969 (1974).
[26] D. G. Leopold, R. J. Hemley, and V. Vaida, J. Chem. Phys. **75**, 4758 (1981).
[27] L. Goodman and I. Ozkan, Chem. Phys. Lett. **61**, 216 (1979).
[28] C. Mijoule and P. Yvan, Chem. Phys. Lett. **43**, 524 (1976); J. E. Ridley and M. C. Zerner, J. Mol. Spectrosc. **76**, 71 (1979).
[29] V. Molina and M. Merchán, J. Phys. Chem. A **105**, 3745 (2001).
[30] W.-H. Fang and D. L. Phillips, ChemPhysChem **3**, 889 (2002).
[31] Y.-W. Wang, H.-Y. He, and W.-H. Fang, J. Mol. Struct.: THEOCHEM **634**, 281 (2003).
[32] R. K. Kakar, E. A. Rinehart, C. R. Quade, and T. Kojima, J. Chem. Phys. **52**, 3803 (1970).
[33] K. B. Borisenko, C. W. Bock, and I. Hargittai, J. Phys. Chem. **100**, 7426 (1996).
[34] V. S. Antonov, V. S. Letokhov, and A. N. Shibanov, Appl. Phys. **22**, 293 (1980).
[35] S. R. Long, J. T. Meek, P. J. Harrington, and J. P. Reilley, J. Chem. Phys. **78**, 3341 (1983).
[36] J. J. Yang, D. A. Gobeli, and M. A. El-Sayed, J. Phys. Chem. **89**, 3426 (1985).
[37] J. J. Yang, D. A. Gobeli, R. S. Pandolfi, and M. A. El-Sayed, J. Phys. Chem. **87**, 2255 (1983).
[38] A. V. Polevoi, V. M. Matyuk, G. A. Grigor'eva, and V. K. Potapov, Khim. Vys. Energ. **18**, 195 (1984).
[39] C. R. Silva and J. P. Reilley, J. Phys. Chem. A **101**, 7934 (1997).
[40] L. Zhu and T. J. Cronin, Chem. Phys. Lett. **317**, 227 (2000).
[41] V. S. Antonov, I. N. Knyazev, V. S. Letokhov, V. M. Matyuk, V. G. Movshev, and V. K. Potapov, Khim. Vys. Energ. **12**, 476 (1978); V. S. Antonov and V. S. Letokhov, Appl. Phys. **24**, 89 (1981); V. S. Antonov, Opt. Spektrosk. **52**, 10 (1982).
[42] M. A. Grela and A. J. Colussi, J. Phys. Chem. **90**, 434 (1986).
[43] J. A. Warren and E. R. Bernstein, J. Chem. Phys. **85**, 2365 (1986).
[44] M. Koyanagi, R. J. Zwarich, and L. Goodman, J. Chem. Phys. **56**, 3044 (1972).
[45] M. Berger and C. Steel, J. Am. Chem. Soc. **97**, 4817 (1975).
[46] A. Inoue, M. Ushiyama, and N. Ebara, Chem. Phys. Lett. **117**, 18 (1985); A. R. Rennert and C. Steel, *ibid.* **78**, 36 (1981); G. A. Zalesskaya, D. L. Yakovlev, and E. G. Sambor, Opt. Spektrosk. **86**, 205 (1999).
[47] Y. Hirata and E. C. Lim, Chem. Phys. Lett. **71**, 167 (1980).
[48] A. P. Darmanyan and C. S. Foote, J. Phys. Chem. **97**, 4573 (1993).
[49] A. P. Baronavski and J. C. Owrutsky, Chem. Phys. Lett. **333**, 36 (2001).
[50] J. Dobkowksi, Z. R. Grabowski, J. Waluk, W. Kühne, W. Rettig, C. Rullière, W. Yang, J. Adamus, and J. Gebicki, Proc. Indian Acad. Sci., Math. Sci. **104**, 143 (1992).
[51] S. Srivistava, E. Yourd, and J. P. Toscano, J. Am. Chem. Soc. **120**, 6173 (1998).
[52] S. Anand, M. M. Zamari, G. Menkir, R. J. Levis, and H. B. Schlegel, J. Phys. Chem. A **108**, 3162 (2004).
[53] H.-Q. Zhao, Y.-S. Cheung, C.-L. Liao, C.-X. Liao, C. Y. Ng, and W.-K. Li, J. Chem. Phys. **107**, 7230 (1997).
[54] R. Srinivasan, V. A. Lobastov, C.-Y. Ruan, and A. H. Zewail, Helv. Chim. Acta **86**, 1763 (2003).
[55] H. Ihee, B. M. Goodson, R. Srinivasan, V. A. Lobastov, and A. H. Zewail, J. Phys. Chem. A **106**, 4087 (2002).
[56] M. Dantus, S. B. Kim, J. C. Williamson, and A. H. Zewail, J. Phys. Chem. **98**, 2782 (1994); J. C. Williamson, J. Cao, H. Ihee, H. Frey, and A. H. Zewail, Nature (London) **386**, 159 (1997).
[57] J. C. Williamson and A. H. Zewail, Chem. Phys. Lett. **209**, 10 (1993).
[58] M. J. Frisch, G. W. Trucks, H. B. Schlegel *et al.*, GAUSSIAN 98 (Gaussian Inc., Pittsburgh, PA, 1998).
[59] M. W. Schmidt, K. K. Baldridge, J. A. Boatz *et al.*, J. Comput. Chem. **14**, 1347 (1993).
[60] A. D. Becke, J. Chem. Phys. **98**, 5648 (1993); R. H. Hertwig and W. Koch, Chem. Phys. Lett. **268**, 345 (1997); P. J. Stephens, F. J. Devlin, C. F. Chabalowski, and M. J. Frisch, J. Phys. Chem. **98**, 11623 (1994).
[61] J. M. Martell, H. Yu, and J. D. Goddard, Mol. Phys. **92**, 497 (1997).
[62] H. Y. Afeefy, J. F. Liebman, and S. E. Stein, in *NIST Chemistry WebBook*, NIST Standard Reference Database Number 69, edited by P. J. Linstrom and W. G. Mallard (National Institute of Standards and Technology, Gaithersburg, MD, 2005).
[63] M. W. Schmidt and M. S. Gordon, Annu. Rev. Phys. Chem. **49**, 233 (1998); B. O. Roos, in *Methods in Computaional Molecular Physics*, edited by G. H. F. Diercksen and S. Wilson (Reidel, Dordrecht, Netherlands, 1983), p. 161.
[64] H. Nakano, J. Chem. Phys. **99**, 7983 (1993).
[65] E. W.-G. Diau, C. Kötting, and A. H. Zewail, ChemPhysChem **2**, 273 (2001).
[66] *Stereochemical Applications of Gas-Phase Electron Diffraction. Part A: The Electron Diffraction Technique*, edited by I. Hargittai and M. Hargittai (VCH, New York, 1988).
[67] A. W. Ross, M. Fink, R. Hilderbrandt, J. Wang, and V. H. Smith, Jr., in *International Tables for Crystallography*, edited by A. J. C. Wilson and E. Prince (Kluwer, Boston, 1999), Vol. C, p. 262.
[68] V. S. Mastryukov and S. J. Cyvin, J. Mol. Struct. **29**, 15 (1975); V. S. Mastryukov, E. L. Osina, L. V. Vilkov, and S. J. Cyvin, Zh. Strukt. Khim. **17**, 80 (1976); E. L. Osina, V. S. Mastryukov, L. V. Vilkov, and S. J. Cyvin, *ibid.* **16**, 1065 (1975).
[69] D. Shorokhov, S. T. Park, and A. H. Zewail, ChemPhysChem **6**, 2228 (2005).
[70] M. M. Lin, D. Shorokhov, and A. H. Zewail, Chem. Phys. Lett. **420**, 1 (2006).
[71] J. C. Williamson and A. H. Zewail, J. Phys. Chem. **98**, 2766 (1994); J. S. Baskin and A. H. Zewail, ChemPhysChem **6**, 2261 (2005).
[72] W. H. Press, S. A. Teukolsky, W. T. Vetterling, and B. P. Flannery, *Numerical Recipes in C: The Art of Scientific Computing* (Cambridge University Press, Cambridge, 1999).
[73] J. R. Taylor, *An Introduction to Error Analysis. The Study of Uncertainties in Physical Measurements*, 2nd ed. (University Science Books, Sausilito, 1997).
[74] R. J. Mawhorter, M. Fink, and B. T. Archer, J. Chem. Phys. **79**, 170 (1983).
[75] K. A. Holbrook, M. J. Pilling, and S. H. Robertson, *Unimolecular Reactions*, 2nd ed. (Wiley, New York, 1996).
[76] J. G. Calvert and J. N. Pitts, Jr., *Photochemistry* (Wiley, New York, 1967); A. Horowitz and J. G. Calvert, J. Phys. Chem. **86**, 3105 (1982); A. Horowitz, C. J. Kershner, and J. G. Calvert, *ibid.* **86**, 3094 (1982); J. S. Yadav and J. D. Goddard, J. Chem. Phys. **84**, 2682 (1986); B. F. Gherman, R. A. Friesner, T.-H. Wong, Z. Min, and R. Bersohn, *ibid.* **114**, 6128 (2001); Y. Kurosaki and K. Yokoyama, Chem. Phys. Lett. **371**, 568 (2003).
[77] R. G. W. Norrish, H. G. Crone, and O. D. Saltmarsh, J. Chem. Soc. 1456

(1934); Y. Haas, Photochem. Photobiol. Sci. **3**, 6 (2004).
[78] W.-K. Chen, J.-W. Ho, and P.-Y. Cheng, J. Phys. Chem. A **109**, 6805 (2005); W.-K. Chen and P.-Y. Cheng, *ibid.* **109**, 6818 (2005).
[79] A. B. Burrill, J. T. Zhou, and P. M. Johnson, J. Phys. Chem. A **107**, 4601 (2003).
[80] D. G. Wilden and J. Comer, J. Phys. B **13**, 627 (1980).
[81] P. Swiderek, M. Michaud, and L. Sanche, J. Chem. Phys. **105**, 6724 (1996).
[82] E. Yamamoto, T. Yoshidome, T. Ogawa, and H. Kawazumi, J. Electron Spectrosc. Relat. Phenom. **63**, 341 (1993).